1 **Quantifying spatiotemporal variability in zooplankton dynamics in the Gulf of Mexico with**

2 **a physical-biogeochemical model**

4 Taylor A Shropshire[1,2], Steven L Morey[3], Eric P Chassignet[1,2], Alexandra Bozec[1,2], Victoria J

5 Coles[4], Michael R Landry[5], Rasmus Swalethorp[5], Glenn Zapfe[6], Michael R Stukel[1,2]

7 [1]Department of Earth Ocean and Atmospheric Sciences, Florida State University, Tallahassee, FL 32303

8 [2]Center for Ocean-Atmospheric Prediction Studies, Florida State University, Tallahassee, FL

9 [3]School of the Environment, Florida A&M University, Tallahassee, FL

10 [4]University of Maryland Center for Environmental Science, PO Box 775 Cambridge MD 21613

11 [5]Integrative Oceanography Division, Scripps Institution of Oceanography, 8622 Kennel Way, La Jolla, CA 92037

12 [6]University of Southern Mississippi, Division of Coastal Sciences, Hattiesburg, MS, 39406

14 Correspondence: Taylor A. Shropshire (tshropshire@fsu.edu)

15 In preparation for: Biogeosciences

Abstract

Zooplankton play an important role in global biogeochemistry, and their secondary production supports valuable fisheries of the world's oceans. Currently, zooplankton standing stocks cannot be estimated using remote sensing techniques. Hence, coupled physical-biogeochemical models (PBMs) provide an important tool for studying zooplankton on regional and global scales. However, evaluating the accuracy of zooplankton biomass estimates from PBMs has been a major challenge due to sparse observations. In this study, we configure a PBM for the Gulf of Mexico (GoM) from 1993-2012 and validate the model against an extensive combination of biomass and rate measurements. Spatial variability in a multi-decadal database of mesozooplankton biomass for the northern GoM is well resolved by the model with a statistically significant ($p < 0.01$) correlation of 0.90. Mesozooplankton secondary production for the region averaged 66 ± 8 x 10^6 kg C yr^{-1}, equivalent to ~10% of net primary production (NPP), and ranged from 51 to 82 x 10^6 kg C yr^{-1}, with higher secondary production inside cyclonic eddies and substantially reduced secondary production in anticyclonic eddies. Model results from the shelf regions suggest that herbivory is the dominant feeding mode for small mesozooplankton (<1-mm) whereas larger mesozooplankton are primarily carnivorous. In open-ocean oligotrophic waters, however, both mesozooplankton groups show proportionally greater reliance on heterotrophic protists as a food source. This highlights an important role of microbial and protistan food webs in sustaining mesozooplankton biomass in the GoM, which serves as the primary food source for early life stages of many commercially important fish species, including tuna.

1.   Introduction

Within marine pelagic ecosystems, zooplankton function as an important energy pathway between the base of the food chain and higher trophic levels such as fish, birds, and mammals (Landry et al., 2019; Mitra et al., 2014). Zooplankton also have a well-documented impact on chemical cycling in the ocean (Buitenhuis et al., 2006; Steinberg and Landry, 2017; Turner, 2015). The ecological roles of zooplankton, however, are varied and taxon dependent. Globally, protistan grazing is the largest source of phytoplankton mortality, accounting for 67% of daily phytoplankton growth (Landry and Calbet, 2004). Protistan zooplankton function primarily within the microbial loop leading to efficient nutrient regeneration in the surface ocean (Sherr and Sherr, 2002; Strom et al., 1997). By contrast, mesozooplankton contribute significantly less to phytoplankton grazing pressure, consuming an estimated 12% of primary production globally (Calbet, 2001), but strongly impact the biological carbon pump. In addition to grazing pressure on phytoplankton, mesozooplankton affect the biological carbon pump through top-down pressure on protistan grazers, production of sinking fecal pellets, consumption of sinking particles, and active carbon transport during diel vertical migration (Steinberg and Landry, 2017; Turner, 2015). Herbivorous mesozooplankton are particularly important to study as they are often associated with shorter food chains that enable efficient energy transfer from primary producers to higher trophic levels of immediate societal interest such as economically valuable fish species and/or their planktonic larvae.

Zooplankton populations have been identified as being vulnerable to impacts of a warming ocean (Caron and Hutchins, 2013; Pörtner and Farrell, 2008; Straile, 1997), through direct temperature effects on metabolic rates (Ikeda et al., 2001; Kjellerup et al., 2012) and thermal stratification-driven alterations in food web structure and productivity (Landry et al., 2019; Richardson, 2008). Studies aimed at monitoring and predicting zooplankton populations are therefore critical for understanding the first-order effects of a warming ocean on marine ecosystems given the importance of secondary production and the impact zooplankton have on biogeochemical cycling. Despite their importance, zooplankton have been historically sampled with limited temporal and spatial resolution. Unlike ocean hydrodynamics and phytoplankton variability, zooplankton abundance cannot currently be estimated remotely from space. Thus, numerical models provide a useful tool for synoptic assessments of zooplankton stocks on basin and global scales (Buitenhuis et al., 2006; Sailley et al., 2013; Werner et al., 2007). Nonetheless, evaluating the accuracy of

67 zooplankton abundance estimates in numerical experiments, such as three-dimensional physical-
68 biogeochemical ocean models (PBMs), is a major challenge due to the sparse ship-based
69 observations in most regions (Everett et al., 2017). Consequently, PBMs are typically
70 predominately validated against surface chlorophyll (Chl) from remote sensing products (Doney
71 et al., 2009; Gregg et al., 2003; Xue et al., 2013).

72 In most marine environments, phytoplankton net growth rates and biomass are determined
73 primarily by the imbalance between phytoplankton growth and zooplankton grazing (Landry et
74 al., 2009). PBMs can accurately predict phytoplankton standing stock (i.e. compare well with
75 satellite Chl observations) despite being driven by the wrong underlying dynamics, leading to
76 major errors in model estimates of secondary production and nutrient cycling (Anderson, 2005;
77 Franks, 2009). For instance, parameter tuning using only surface Chl as a validation metric can
78 allow broad patterns in phytoplankton biomass to be reproduced even with gross over- or
79 underestimation of phytoplankton turnover times. Similarly, even a model that is validated against
80 satellite Chl and net primary production might completely misrepresent the proportion of
81 phytoplankton mortality mediated by zooplankton groups, leading to inaccurate estimates of
82 important ecological metrics like secondary production and carbon export. Hence, validating
83 PBMs against zooplankton dynamics is key to increasing confidence in model solutions. The
84 importance of validation is further evident when considering zooplankton impacts on the behaviors
85 of biogeochemical models (Everett et al., 2017). Differences in simulated zooplankton
86 communities expressed through the number of functional types, various mathematical grazing
87 functions, or the arrangement of transfer linkages have been shown to have substantial impacts on
88 the dynamics of simple and complex biogeochemical models (Gentleman et al., 2003b; Gentleman
89 and Neuheimer, 2008; Mitra et al., 2014; Murray and Parslow, 1999; Sailley et al., 2013).

90 The Gulf of Mexico (GoM) is a particularly suitable region for examining zooplankton dynamics
91 with PBMs. In the northern and central Gulf, zooplankton abundances have been extensively
92 measured for over three decades (1982-present) by the Southeast Area Monitoring and Assessment
93 Program (SEAMAP). Within the SEAMAP dataset, zooplankton biomass exhibits strong
94 spatiotemporal variability, reflecting complex physical circulation in the GoM. Circulation off the
95 shelf is characterized by substantial upper layer mesoscale activity driven primarily by the
96 energetic Loop Current (Forristall et al., 1992; Maul and Vukovich, 1993; Oey et al., 2005). In

97 contrast, coastal and shelf circulation patterns are predominantly wind-driven (Morey et al., 2003a,

98 2013). Freshwater discharged by the Mississippi River and other smaller rivers is frequently

99 entrained offshore by shelf break interaction with mesoscale features (e.g., anti-cyclonic loop

100 current eddies), leading to strong horizontal and vertical gradients in physical and biogeochemical

101 quantities (Morey et al., 2003b). Overlap of these gradients with the SEAMAP study region result

102 in zooplankton collections across biogeochemically heterogeneous environments, providing a

103 powerful model constraint. For instance, Chl ranges across three orders-of-magnitude (~0.01 – 10

104 mg Chl m^{-3}) from oligotrophic to eutrophic waters.

105 Over the past decade several PBM studies have been conducted in the GoM, all primarily

106 examining nutrient and phytoplankton dynamics. Early work by Fennel et al. (2011) examined

107 phytoplankton dynamics on the Louisiana and Texas continental shelf, concluding that loss terms

108 (e.g., grazing) rather than growth rates dictated accumulation rates of phytoplankton biomass. With

109 the same biogeochemical model, Xue et al. (2013) conducted the first gulf-wide PBM study to

110 investigate broad seasonal biogeochemical variability and to constrain a shelf nitrogen budget.

111 More recently, Gomez et al. (2018) implemented a biogeochemical model with multiple

112 phytoplankton and zooplankton functional types to gain a more detailed understanding of nutrient

113 limitation and phytoplankton dynamics in the GoM. To examine phytoplankton seasonality and

114 biogeography in the oligotrophic Gulf, Damien et al. (2018) validated a PBM based on a unique

115 subsurface autonomous glider dataset. Together, these studies have demonstrated the utility of

116 PBMs for investigating GoM lower trophic levels and have also highlighted the key ecosystem

117 roles of zooplankton. Specifically, both Fennel et al. (2011) and Gomez et al. (2018) identified the

118 importance of zooplankton in modulating the simulated seasonal patterns of phytoplankton

119 biomass, emphasizing the importance of top-down control on the shelf. Although simulated

120 zooplankton community results were not presented, Damien et al. (2018) noted that biotic

121 processes such as grazing pressure, are "essential to fully understanding the functioning of the

122 GoM ecosystem." However, in all of these studies, zooplankton validation was largely absent.

123 In this study, we configured a PBM for the GoM to estimate zooplankton abundance and analyze

124 zooplankton community dynamics. The PBM is forced by three-dimensional hydrodynamic fields

125 from a data assimilative Hybrid Coordinate Ocean Model (HYCOM) hindcast of the GoM

126 (http://www.hycom.org)and is based on the biogeochemical model NEMURO (North Pacific

127 Ecosystem Model for Understanding Regional Oceanography; Kishi et al., 2007), which is

128 substantially modified here for application to the GoM. The model is integrated over 20-years

129 (1993-2012) and validated against an extensive combination of remote and in situ measurements

130 including total and size-fractioned mesozooplankton biomass and grazing rates, microzooplankton

131 grazing rates, phytoplankton growth rates and net primary production as well as validation of

132 surface chlorophyll and vertical profiles of chlorophyll and nitrate. Our goals were: 1) to develop

133 and validate a PBM to estimate mesozooplankton abundance, 2) to characterize the spatiotemporal

134 variability in mesozooplankton dietary composition, and 3) to quantify regional mesozooplankton

135 secondary production. We focus primarily on the oligotrophic open-ocean GoM, where prey (i.e.

136 zooplankton) availability may be limiting for fish, their larvae and other higher trophic levels.

137 **2 Methods and data**

138 **2.1 Biogeochemical model configuration**

139 **2.1.1 NEMURO model description**

140 The biogeochemical model for this study is based on NEMURO (Kishi et al., 2007) but has been

141 modified and parameterized to more accurately reflect the ecology of the GoM (herein called

142 NEMURO-GoM). NEMURO is a concentration-based, lower-trophic-level ecosystem model

143 originally developed and parameterized for the North Pacific. Like most marine functional-group

144 biogeochemical models, it is structured around simplified representations of the lower food web

145 originating from earlier nutrient-phytoplankton-zooplankton models (Fasham et al., 1990; Franks,

146 2002; Riley, 1946). Complexity is added through additional state variables and transfer functions

147 with the specific goal of resolving dynamics within the nutrient, phytoplankton and zooplankton

148 pools. In total, NEMURO has eleven state variables: six non-living state variables – nitrate (NO_3),

149 ammonium (NH_4), dissolved organic nitrogen (DON), particulate organic nitrogen (PON), silicic

150 acid ($Si(OH)_4$) and particulate silica (Opal); two phytoplankton state variables – small (SP) and

151 large phytoplankton (LP); and three zooplankton state variables – small (SZ), large (LZ) and

152 predatory zooplankton (PZ).

153 Each biological state variable in NEMURO is an aggregated representation of taxonomically

154 diverse plankton groups that function similarly in the ecosystem. The phytoplankton community

155 is modeled as two functional types of obligate autotrophs: small phytoplankton (SP, predominantly

156 cyanobacteria and picoeukaryotes in the GoM) and large phytoplankton (LP, diatoms). Small

zooplankton (SZ) represent heterotrophic protists, and metazoan zooplankton are divided into suspension-feeding mesozooplankton (LZ) and predatory zooplankton (PZ). Here, we assume that LZ and PZ are non-migratory. Heterotrophic bacteria are implicitly represented by temperature-dependent decomposition rates, which represent nitrification and remineralization processes. NEMURO uses nitrogen as a model "currency" since it is the major limiting macronutrient in much of the ocean. Silica is also included as a potentially co-limiting nutrient for diatoms (i.e. LP).

By default, sinking in NEMURO is restricted to PON and Opal, and benthic processes are not included. Here, because of the large shelf area in the GoM, we implemented a simple diagenesis of PON/Opal to NO_3/SiO_4 and removal of PON/Opal through sedimentation, where 1% of the flux sinking out of bottom cell was removed and 10% converted back into NO_3/SiO_4. However, we found that this had no significant impact on the simulated surface Chl or mesozooplankton biomass on the shelf. The inclusion of a more complex sediment diagenesis model (including denitrification) would have added further realism (Fennel et al., 2011). However, our main focus was to evaluate zooplankton dynamics in the oligotrophic region where higher trophic levels that depend on mesozooplankton secondary production may experience food limitation and where benthic processes are negligible.

NEMURO was chosen for the present study because it distinguishes SZ, LZ and PZ, permitting a detailed analysis of dynamics for multiple functional types in the GoM zooplankton community. During initial GoM simulations, default NEMURO parameterizations, configured for the North Pacific (Kishi et al., 2007), substantially overestimated surface nitrate, surface Chl, and mesozooplankton biomass relative to observations. We attribute these differences to: 1) substantially higher temperatures in the GoM compared with the North Pacific, which significantly increase decomposition and growth rates in the model resulting in higher nutrient recycling and elevated near-surface stocks of phytoplankton and zooplankton, and 2) distinct differences in taxonomic composition of phytoplankton and zooplankton communities in the GoM and North Pacific, with significant differences in key parameter values associated with growth and grazing.

For more details on the specific processes represented and the interactions between state variables in NEMURO, we direct readers to Kishi et al. (2007). All model equations are provided in the supplement to this manuscript. Biogeochemical model forcing, initial and open boundary

186 conditions are also outlined in Supplement **S1**. Briefly, daily average shortwave radiation fields
187 obtained from Climate Forecast System Reanalysis (CFSR) were used to force light limitation of
188 phytoplankton. Once a final parameter set was determined (see section 2.1.3), initial and open
189 boundary conditions for all state variables were prescribed from a spun up idealized one-
190 dimensional version of NEMURO-GoM. After initializing, the three-dimensional model was spun
191 up over four years before conducting the full 20-year experiment. River nutrient input from the
192 Mississippi was prescribed using nitrate samples collected by United States Geological Survey
193 (USGS) and due to a lack of observations for other rivers was prescribed for all 37 rivers
194 represented in the model.

195 **2.1.2   Modifications to default NEMURO model**
196 To improve realism for application to the GoM, five structural changes were made to the original
197 NEMURO model. First, we removed the SP to LZ grazing pathway. The original SP state variable
198 for the North Pacific represents nanophytoplankton (e.g. coccolithophores), which can be
199 important prey of copepods and other mesozooplankton. In the GoM, however, cyanobacteria and
200 picoeukaryotes (too small for direct feeding by most mesozooplankton) comprise much of the
201 phytoplankton biomass and hence are represented as SP in our model. In addition to adding
202 ecological realism, this change in direct trophic connection between SP and LZ allowed the model
203 to produce a more realistic LP-dominated phytoplankton community on the shelf (see Discussion).

204 Next, quadratic mortality was replaced with linear mortality for all biological state variables with
205 the exception of predatory zooplankton (PZ). In biogeochemical models, quadratic mortality is
206 often used for numerical stability and/or to represent implicit loss terms to an un-modeled parasite
207 or predator that covaries in abundance with its prey (e.g. viral lysis of phytoplankton or predation
208 by un-modeled higher predators) (Anderson et al., 2015). However, grazing mortality is explicitly
209 modeled in NEMURO and viral mortality is generally not a substantial loss term for bulk
210 phytoplankton (Staniewski and Short, 2018). Quadratic mortality was retained for PZ, to account
211 for predation pressure of un-modeled predators (e.g. planktivorous fish). During the model tuning
212 process, we found that removal of quadratic mortality from the four other plankton functional
213 groups was an important parameterization change that allowed the model to simulate more realistic
214 mesozooplankton biomass in the oligotrophic GoM (see Discussion).

The default ammonium inhibition term and light limitation functional form in NEMURO were replaced in NEMURO-GoM with more widely adopted parameterizations. The exponential ammonium inhibition term in the nitrate limitation function was replaced with the term described by Parker (1993), as has been done in previous PBM studies (Fennel et al., 2006) due to the non-monotonic behavior of the default NEMURO ammonium inhibition term. At high NO_3 concentrations, the default term is known to generate unrealistic phytoplankton nutrient uptake patterns in which total nutrient uptake (i.e. uptake of NO_3 + uptake of NH_4) can actually decrease despite increases in NH_4 (and constant NO_3).

Light limitation in NEMURO is based on an optimal light parameterization that implicitly includes photoinhibition. This formulation was replaced with the Platt et al. (1980) functional form that allows one to explicitly control the amount of photoinhibition, which can be important in the GoM where surface irradiances are high. Additionally, the Platt functional form is commonly used and thus parameter values are easier to find for comparison (e.g. initial slope of the PI curve (α)). This formulation is also implemented in newer versions of NEMURO, such as the code used in the Regional Ocean Modeling System (ROMS) NEMURO biogeochemical package.

Finally, to account for photoacclimation and more accurately simulate Deep Chlorophyll Maximum (DCM) dynamics, we replaced the constant C:Chl parameter with a variable C:Chl model where ratios for SP and LP were allowed to vary based on the formulation described by Li et al. (2010), which considers both light and nutrient limitation (see Supplemental). The Li et al. (2010) equations build on a previously constructed dynamic regulatory model of phytoplankton physiology which describes C:Chl variability under balanced growth and nutrient saturated conditions at constant temperature (see Geider et al., 1998)). Herein, "default" NEMURO includes the modified ammonium inhibition, light formulation, and variable C:Chl model.

2.1.3 NEMURO-GoM model tuning procedure

In total, NEMURO includes 71 parameters, 23 of which were modified in the present study. For initial model tuning, we used an idealized one-dimensional model designed to mimic the oligotrophic GoM. To guide our tuning procedure, we relied on a semi-quantitative approach where the one-dimensional model solution was evaluated based on five ecosystem benchmarks. Target values for benchmarks and other ecosystem attributes were determined from observations

244 or a theoretical basis. Ecosystem benchmarks included: surface Chl, mesozooplankton biomass,

245 DCM depth, DCM magnitude, and SP:LP ratio. Surface Chl and mesozooplankton biomass were

246 chosen as benchmarks to evaluate the realism of plankton biomass in the model. The DCM depth

247 and magnitude were chosen to evaluate the vertical structure of the simulated ecosystem, and

248 SP:LP ratio was used to gauge the realism of the plankton community composition (i.e. high SP:LP

249 is expected in the oligotrophic GoM). The model was also tuned by considering the relative

250 magnitudes of loss terms for phytoplankton (grazing, mortality, respiration, and excretion), total

251 protistan zooplankton grazing relative to mesozooplankton grazing, as well as surface and deep

252 nitrate concentrations. We outline each parameter change, justification and the resulting impact on

253 the ecosystem benchmarks simulated by the idealized one-dimensional model in Supplement **S3**.

254 Where possible, we modified parameters in groups so that relative changes were consistent

255 throughout the model (e.g. doubling all zooplankton mortality terms). After tuning in the one-

256 dimensional model, parameter sets were implemented into the full three-dimensional model where

257 additional tuning was performed. Once a final parameter set was determined we conducted a

258 parameter sensitivity analysis over 18 individual experiments to identify impacts of parameter

259 changes from default NEMURO values (**S4**).

260 **2.2   Physical model configuration**

261 **2.2.1   Description of the offline numerical environment**

262 To run large numbers of three-dimensional simulations efficiently for basin-scale tuning,

263 NEMURO-GoM was run offline using the MITgcm offline tracer advection package. MITgcm

264 was selected as it contains convenient packages for running offline simulations (McKinley et al.,

265 2004). That is, the dynamical equations of motion are not computed during the NEMURO-GoM

266 integration, but rather the physical prognostic variables (i.e., temperature, salinity and three-

267 dimensional velocity fields) are prescribed from daily-averaged flow fields saved from a previous

268 hydrodynamic model integration. This allows the recycled use of flow fields leaving only the tracer

269 equations to be computed. In the offline MITgcm package, the prognostic variables provide input

270 to an advection scheme and mixing routine that conservatively handles offline advection and

271 diffusion of the biogeochemical tracer fields. MITgcm has many options for linear and non-linear

272 advection schemes. Here we use a 3rd order direct space time flux limiting scheme. Sub grid-scale

273 mixing of the biogeochemical fields is handled offline through the nonlocal K-Profile

274 Parameterization (KPP) package based on mixing schemes developed by Large et al. (1994). For

275 more information about the MITgcm packages, we direct readers to the MITgcm manual

276 (http://mitgcm.org/).

277 There are two main advantages to running PBMs in an offline environment: 1) the momentum

278 equations are not integrated during the model run; and 2) the physical time step is no longer bound

279 by the dynamical Courant–Friedrichs–Lewy (CFL) numerical stability criterion, which together

280 significantly reduces the computational cost. Instead, the stability of the tracer advection scheme

281 and time scales needed to resolve biological/physical processes of interest set the limits on the time

282 steps and prescription frequencies of flow fields. When the physical time step is shorter than the

283 flow field prescription frequency, a simple linear interpolation of the flow fields is performed

284 between time steps. Offline simulations of tracer advection have been found to closely resemble

285 online runs (that is, computed together with the integration of the hydrodynamic model's

286 prognostic equations) when the three-dimensional flow fields are prescribed at a frequency that is

287 at or below the inertial period ($T = 2\pi/f$, $T_{GoM} > 24\ hr$) for a region (Hill et al., 2005).

288 In the present study, the offline time step (30 minutes) is an order of magnitude greater than the

289 hydrodynamic model's (HYCOM-GoM, described in Section 2.2.2) baroclinic time step (120

290 seconds). For reference, HYCOM-GoM required ~76 days to run to completion on 64 parallel

291 cores. These time requirements would increase considerably with the 11 additional

292 biogeochemical tracers used in NEMURO. In contrast, NEMURO-GoM ran significantly faster,

293 taking a total of ~50 hours on 80 parallel cores. Offline models offer a valuable tool for integrating

294 PBMs particularly as spatial resolution and complexity in these models continues to increase (e.g.,

295 DARWIN (Follows et al., 2007), GENOME (Coles et al., 2017)). While computationally

296 advantageous, however, offline simulations have inherently greater input and output (I/O)

297 demands that can become bottlenecks in some applications. Issues with conservation can also arise

298 as three-dimensional advection schemes are only approximately positive definite.

299 **2.2.2 Description of the offline dynamical fields**

300 The NEMURO-GoM model is "forced" by daily averaged three-dimensional velocity, temperature

301 and salinity fields from a pre-existing 20-year (1993-2012) HYCOM (HYbrid Coordinate Ocean

302 Model) (Chassignet et al., 2003) regional GoM hindcast (H-GoM). H-GoM is based on version

303 2.2.99B of the HYCOM code, originally provided by the Naval Oceanographic Office

304 (NAVOCEANO) Major Shared Resource Center. H-GoM was run at $1/25^{th}$ degree (~4 km)

305 horizontal resolution with 36 vertical hybrid coordinate layers and assimilated historic, in situ and

306 satellite observations. The domain encompasses the entire GoM and extends south of the Mexican-

307 Cuba Yucatan channel to 18 °N and as far east as 77 °W (**Fig. 1**). Further details on H-GoM

308 (experiment ID: GOMu0.04/expt_50.1), including model forcing and the main model

309 configuration file (i.e. blkdat.input_501), can be found at https://www.hycom.org.

310 The H-GoM flow fields were mapped from the HYCOM native hybrid vertical coordinate to z-

311 levels used by the MITgcm. NEMURO-GoM was configured for 29 vertical z-levels (10-m

312 intervals from 0-150 m, 25-m intervals from 150-300 m, 50-m intervals from 300-500m, and 1000

313 m, 2000 m, ~4000 m). Mapping was performed by computing total zonal and meridional

314 transports across the lateral boundaries of each MITgcm grid cell (e.g., 0-10 m bin; which may

315 include multiple HYCOM layers) and then dividing by the area of the respective cell face. This

316 vertical mapping approach is consistent as both HYCOM and MITgcm use an Arakawa C-grid

317 orientation for model variables. The H-GoM bathymetry was adjusted such that no partial cells

318 existed in the domain to avoid thin cells. The continuity equation was subsequently used to

319 calculate vertical velocities. The use of transports in this approach ensures conservation and

320 approximately identical profiles of vertical velocity to those in H-GoM fields. For mapping of

321 temperature and salinity fields (used in the KPP mixing routine and for scaling biological

322 temperature dependent rates), a simple linear interpolation was performed.

323 **2.3   Model validation**

324 **2.3.1   Surface chlorophyll observations**

325 A benchmark for surface Chl was determined using the Sea-Viewing Wide Field-of-View Sensor

326 (SeaWIFS) product from the Ocean Biology Processing Group (OBPG) of the National

327 Aeronautics and Space Administration (NASA). The product used here is the mapped, level-3,

328 daily, 9-km resolution images from 4 September 1997 to 10 December 2010 processed according

329 to the algorithm of Hu et al. (2012). To compute model-data point-to-point comparisons, we take

330 the corresponding daily-averaged simulated surface Chl field and interpolate to the SeaWIFS grid

331 before applying the daily cloud coverage mask corresponding to the matching SeaWIFS image. In

332 total 4,291 daily images consisting of 22,244,513 non-zero cell values (herein referred to SeaWIFS

measurements) were used to validate NEMURO-GoM. Approximately 500-1200 daily model-data point-to-point comparisons were made for each SeaWIFS grid cell (**Fig 1**).
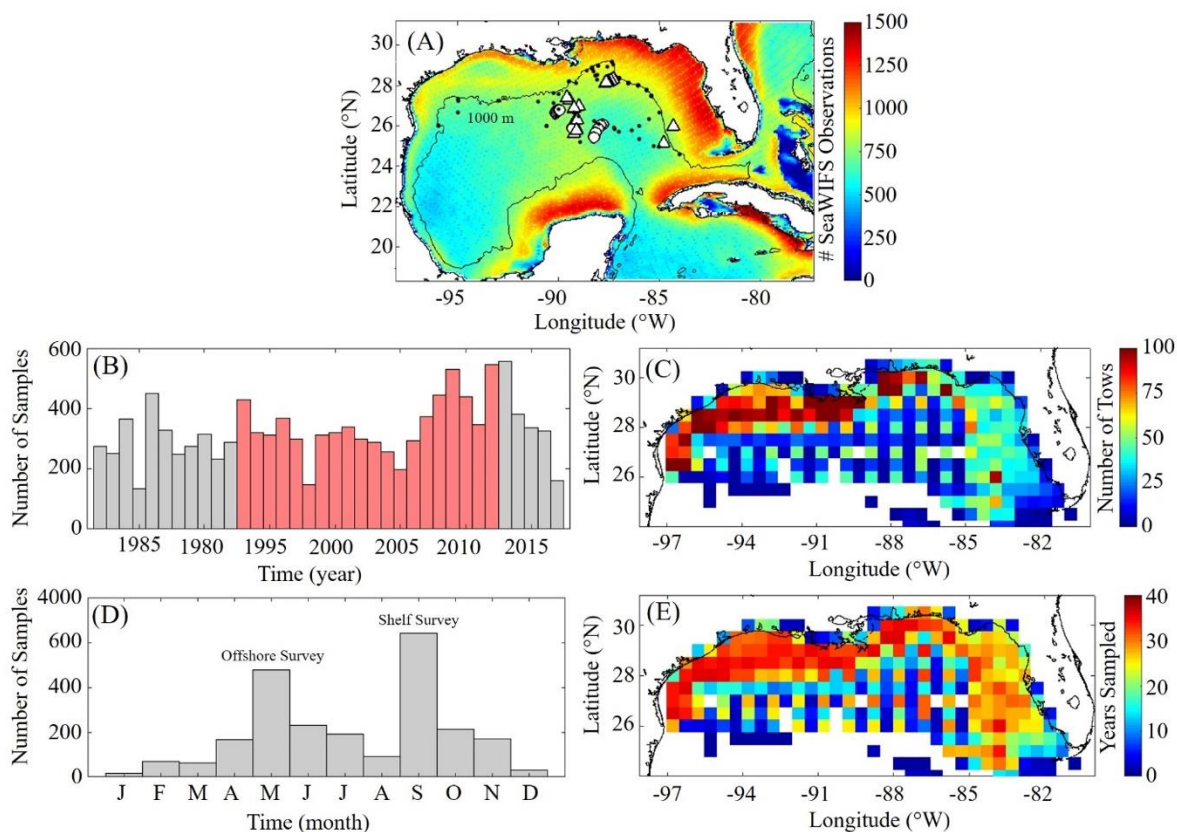
Figure 1 (A-E): Spatial and temporal coverage of observational data sets used for model validation. Total number of non-zero values available in daily SeaWIFS images from September 1997 to 10 December, 2010 along with nitrate profiles from the World Ocean Database (black dots) and the location of in situ measurements collected during May 2017 (circles) and May 2018 (triangles) process study cruises (A). Total annual sampling of the SEAMAP surveys from 1983-2017 with samples overlapping with the PBM simulation period denoted in red (B). Samples organized by month (D). Total sample density within each 0.5° x 0.5° box (C) along with the number of years with at least one sample (E). 1000 m isobaths and coastline are denoted by black continuous lines.

2.3.2 Mesozooplankton biomass observations

To evaluate model mesozooplankton biomass estimates, we used plankton tows collected during Southeast Area Monitoring and Assessment Program (SEAMAP) surveys in the northern and

348 central GoM. In total, 11,781 plankton tows were collected from 1983-2017, with two main annual

349 surveys in the spring (offshore) and fall (shelf) (**Fig. 1**). On average, SEAMAP collected

350 approximately 300 samples per year with a specific sampling array offshore and more general

351 sampling coverage on the shelf. In total, 6,835 samples were used for direct point-to-point model-

352 data comparisons. Samples were collected using standard gear consisting of a 61-cm diameter

353 bongo frame fitted with two 333-μm mesh nets. The nets were fished in a double-oblique tow

354 pattern from the surface down to 200 m or 5 m off the bottom and back to the surface. Simultaneous

355 samples were also collected using a 202-μm mesh net during 82 tows. Of these samples, roughly

356 half were collected in the oligotrophic GoM. The average ratio between biomass measured in the

357 333- and 202-μm bongo tows (0.5093 ± 0.12) was used to convert 333-μm samples so that direct

358 comparisons could be made with model mesozooplankton (LZ+PZ) biomass fields. Zooplankton

359 biomass was originally quantified as displacement volumes (DV). Carbon mass (CM) equivalents

360 were subsequently calculated as $\log_{10}(CM) = (\log_{10}(DV) + 1.434)/0.820$ (Wiebe, 1988; Moriarty

361 and O'Brien, 2013).

362 For comparison to in situ biomass measurements size ranges were assumed for zooplankton state

363 variables (see section 2.3.4). In NEMURO-GoM, SZ represent heterotrophic protists (e.g. ciliates)

364 and early stages of mesozooplankton, which are typically < 200 μm in the ocean. Hence, SZ are

365 assumed to range in size from 2-200 μm. LZ are considered to represent small mesozooplankton

366 ranging in size from 0.2 to 1.0 mm while PZ represent large mesozooplankton ranging in size from

367 1.0 to 5.0 mm. For comparison to the SEAMAP climatology the model LZ and PZ fields were first

368 converted to units of carbon assuming Redfield C:N ratio and summed over the entire simulation

369 before being depth averaged to the bottom or 200 m. For point-to-point model-data comparisons,

370 total mesozooplankton biomass fields were interpolated to SEAMAP sample locations/times and

371 then depth averaged to the corresponding sample tow depth.

2.3.3   Observed vertical profiles of chlorophyll and nitrate

373 Depth profiles of Chl were also collected during SEAMAP surveys using a SeaBird WETStar

374 fluorometer attached to a CTD. Calibration of the fluorimeter was infrequent, and thus profiles

375 were used to determine the depth of the fluorescence maxima for comparisons to DCM depths in

376 the model. In total, 2,435 profiles were collected from 2003 to 2012, with 1,052 profiles overlying

377 bottom depths >1000 m. Profiles were available for earlier SEAMAP surveys; however, no
378 standard QA/QC protocol for fluorometer data was in place prior to 2003.

379 To evaluate DCM magnitudes in the model, we used 145 fluorescence profiles collected during
380 May 2017 and 2018 process study cruises (see section 2.3.4). The fluorometer was attached to a
381 CTD and calibrated using 126 in situ Chl samples. Chl concentrations were determined from
382 filtered samples collected at depths ranging from 5 to 115 m using High Performance Liquid
383 Chromatography (HPLC). Since the cruise sampling does not overlap with our NEMURO-GoM
384 simulation period, model-data comparisons were made for all 20 years of the model run using
385 sample locations and time of the year. This was also done with other field measurements from the
386 process cruises (see section 2.3.4).

387 For model-data comparisons of nitrate, we utilized profiles from the World Ocean Database
388 (WOD). In total, 96 profiles were available during our simulation period and located in the
389 oligotrophic GoM (>1000 m isobath). Profiles were collected during all months except March and
390 December with the majority of samples collected during May, July and August (**Fig. 1A**).

391 **2.3.4 Biomass and rate measurements from process study cruises**
392 Although in situ rate measurements are made much less frequently than biological standing stock
393 measurements, they offer very powerful constraints for validating the internal dynamics of a
394 biogeochemical model (Franks, 2009). Consequently, we made phytoplankton and zooplankton
395 rate measurements on two cruises in the open ocean GoM in May 2017 and 2018 and used these
396 measurements to validate the model (**Fig. 1A**). On the process study cruises, we utilized a quasi-
397 Lagrangian sampling scheme to investigate plankton dynamics in the oligotrophic GoM. Two
398 drifting arrays (one sediment trap array and one in situ incubation array) were deployed to serve
399 as a moving frame of reference during ~4-day studies ("cycles") characterizing the water parcel
400 (Landry et al., 2009; Stukel et al., 2015). During these cycles, we measured daily profiles of Chl,
401 photosynthetically active radiation, phytoplankton growth rates and productivity, protistan grazing
402 rates, and size-fractionated mesozooplankton biomass and grazing rates.

403 Size-fractionated mesozooplankton biomass and grazing rates were determined from daily day-
404 night paired oblique ring-net tows (1-m diameter, 202-μm mesh). In total, 40 oblique bongo net
405 tows (16 in 2017 and 24 in 2018) sampled the oligotrophic GoM mesozooplankton community

from near surface to a depth ranging from 100-135 m. Upon recovery, the sample was anesthetized using carbonated water, split using a Folsom splitter, filtered through a series of nested sieves (5, 2, 1, 0.5, and 0.2 mm), filtered onto pre-weighed 200-µm Nitex filters, rinsed with isotonic ammonium formate to remove sea salt, and flash frozen in liquid nitrogen. In the lab, defrosted samples were weighed for total wet weight, and subsampled in duplicate (wet weight removed) for gut fluorescence analyses. The remaining wet sample was dried and subsequently reweighed and combusted for CHN analyses to determine total dry weight and C and N biomasses. Gut fluorescence subsamples were homogenized using a sonicating tip, extracted in acetone, and measured for Chl and phaeopigments using the acidification method. The phaeopigment concentrations in the zooplankton guts were the basis for calculated grazing rates using gut turnover times based on temperature relationships for mixed zooplankton assemblages. For additional details, see Décima et al. (2011) and Décima et al. (2016).

Protistan grazing rates were measured using the two-point, "mini-dilution" variant of the microzooplankton grazing dilution method (Landry et al., 1984, 2008; Landry and Hassett, 1982). Briefly, one 2.8-L polycarbonate bottle was gently filled with whole seawater taken from six depths (from the surface to the depth of the mixed layer). A second 2.8-L bottle was then filled with 33% whole seawater and 67% 0.2-µm filtered seawater. Both bottles were then placed in mesh bags and incubated in situ at natural depths for 24 h. These experiments were conducted on each day of the ~4-day cycle. After 24 h, the bottles were retrieved, filtered onto glass fiber filters, and Chl concentrations were determined using the acidification method (Strickland and Parsons., 1972). Net growth rates ($k=\ln(Chl_{final}/Chl_{init})$) in each bottle were determined relative to initial Chl samples. Phytoplankton specific mortality rates resulting from the grazing pressure of protists were calculated as $m = (k_d − k_0)/(1-0.33)$, where k_d is the growth rate in the dilute bottle and k_0 is the growth rate in the control bottle. Phytoplankton specific growth rates were calculated as $\mu = k_0 + m$. For additional details, see Landry et al. (2016) and Selph et al. (2016). Phytoplankton net primary production was quantified at the same depths by $H^{13}CO_3^-$ uptake experiments. Triplicate 2.8-L polycarbonate bottles and a fourth "dark" bottle were spiked with $H^{13}CO_3^-$ and incubated in situ for 24 h at the same sampling depths as for the dilution experiments. Samples were then filtered and the $^{13}C:^{12}C$ ratios of particulate matter determined by isotope ratio mass spectrometry.

3.0   Results

3.1   Surface chlorophyll model-data comparisons

Model surface Chl estimates were found to agree closely with satellite observations reproducing patterns in both the oligotrophic and shelf region (**Fig. 2**). Spatial covariance between SeaWIFS climatology and model surface Chl climatology (calculated with daily cloud cover mask applied) is statistically significant ($p < 0.01$) with a correlation (ρ) of 0.72. When model estimates are compared to all 22,244,513 SeaWIFS measurements at corresponding times and locations (i.e. daily grid cell pairs), we find a ρ value of 0.50 ($p < 0.01$). To facilitate more detailed model-data comparisons, the GoM domain was divided into an oligotrophic region ($\geq$1000 m bottom depth) and a shelf region (<1000 m bottom depth). In the oligotrophic region, the correlation between model-data daily grid cell pairs is significant but weak ($\rho = 0.17$, $p < 0.01$) as a result of relatively low large-scale spatial variability, and hence dominance at the mesoscale. However, bias is quite low (-0.014 mg Chl m^{-3}), equivalent to 10% of the observed mean. In the shelf region, the correlation is higher ($\rho = 0.47$, $p < 0.01$) yet the bias is greater (+0.90 mg Chl m^{-3}), equivalent to 92% of the mean. Previous GoM studies have determined ρ values for monthly averages, which we calculate here for comparison. Based on 30-day averages, the ρ values are 0.70 ($p < 0.01$) for the oligotrophic region and 0.26 ($p < 0.01$) for the shelf region.

In addition to resolving the dominant spatiotemporal variability, the model also captures the amplitude of the seasonal surface Chl signal reasonably well. In the oligotrophic region, the model accurately estimates the observed annual surface Chl minimum (Model: 0.065 ± 0.005 vs. SeaWIFS: 0.065 ± 0.007 mg Chl m^{-3}) while slightly underestimating the observed annual maximum (Model: 0.47 ± 0.15 vs. SeaWIFS: 0.75 ± 0.55 mg Chl m^{-3}). When model estimates for the entire oligotrophic region are taken into account (i.e. not restricted to satellite measurement locations and times), the annual minimum develops in early September, and the maximum develops in late January (**Table 1**). In the shelf region, greater model-data mismatch exists for surface Chl, with the model overestimating the observed annual minimum by 15% (Model: 0.23 ± 0.09 vs. SeaWIFS: 0.20 ± 0.07 mg Chl m^{-3}) and the observed annual maximum by 102% (Model: 8.09 ± 1.31 vs. SeaWIFS: 4.01 ± 1.23 mg Chl m^{-3}). Here, we find the annual surface Chl seasonal cycle almost completely out of phase with the oligotrophic region, with the annual minimum developing in early February and the annual maximum developing at the end of July (**Table 1**).

465
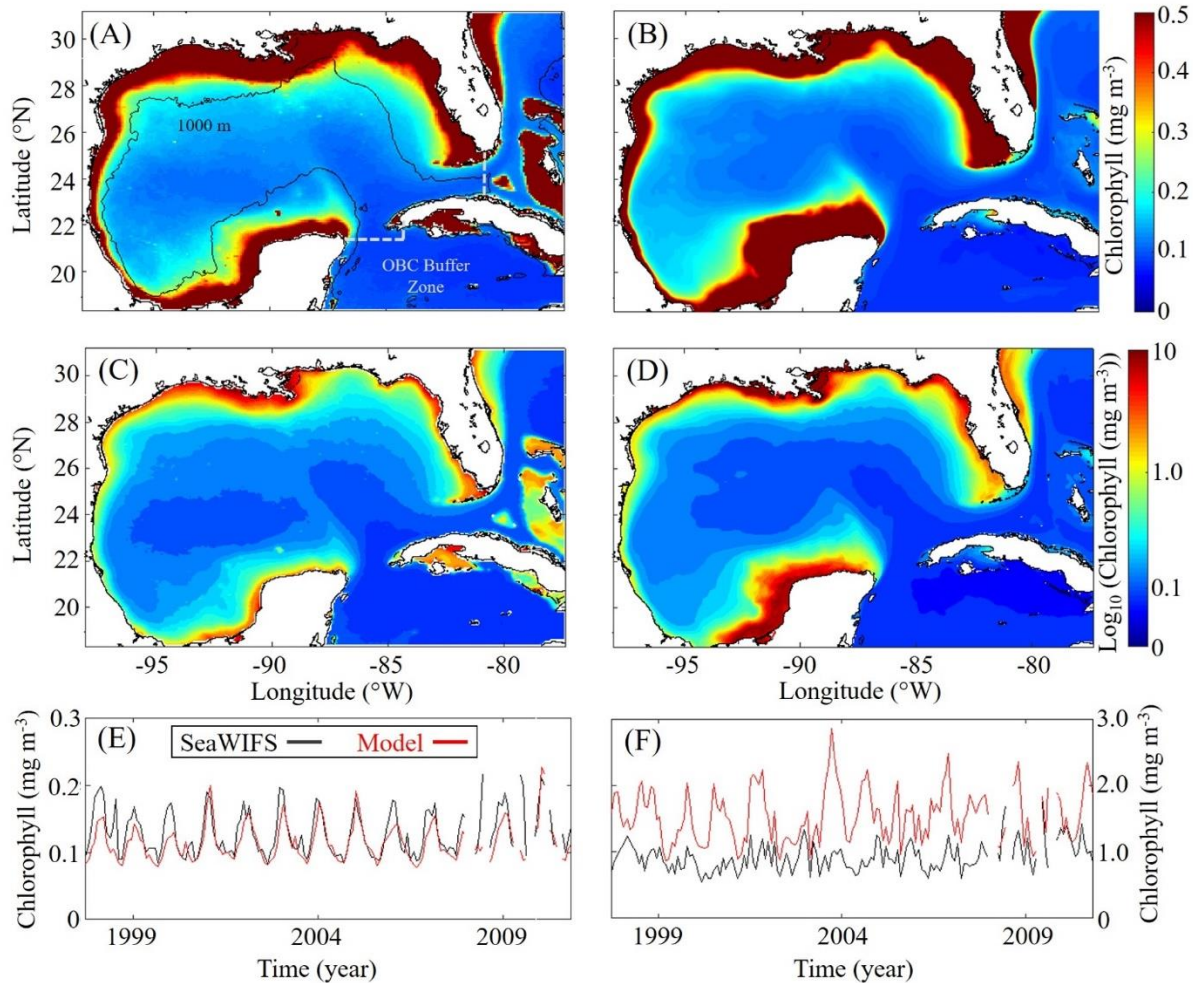
Figure 2 (A-F): Comparison of surface chlorophyll (mg m⁻³) between SeaWIFS observations (left column) and model (right column) from 4 September 1997 to 10 December 2010. Surface chlorophyll climatology computed from daily SeaWIFS images (A) and the corresponding log₁₀ field (C). Surface chlorophyll climatology computed from daily averages over the entire model simulation (1993-2012) (C) and the corresponding log₁₀ field (D). Time series of simulated 30-day average surface chlorophyll based on SeaWIFS observations (black) and model (red) for the oligotrophic region (grid cells with bottom depths ≥1000 m) (E) and shelf region (grid cells with bottom depths <1000 m) (F).

3.2   Regional mesozooplankton biomass model-data comparisons

Model mesozooplankton biomass (i.e. LZ + PZ) fields also agree closely with observations in both the oligotrophic and shelf region (**Fig. 3**). Spatial covariance between SEAMAP climatology and

477 model is statistically significant ($p < 0.01$) with a ρ value of 0.90. When model estimates are

478 compared to SEAMAP tows at corresponding sample times and locations for the 6,835

479 measurements in the simulation period, the ρ value is 0.55 ($p < 0.01$). In the oligotrophic region,

480 the model slightly overestimates mesozooplankton biomass (Model: 4.09 ± 1.82 mg C m^{-3} vs.

481 SEAMAP: 3.52 ± 3.44 mg C m^{-3}) with ρ value of 0.23 ($p < 0.01$) with a bias of 0.57 mg C m^{-3},

482 equivalent to 16% of the observed mean. Conversely, in the shelf region the model underestimates

483 mesozooplankton biomass (Model: 17.40 ± 13.58 mg C m^{-3} vs. SEAMAP: 20.91 ± 24.62 mg C m^{-3}

484), with a ρ value of 0.49 ($p < 0.01$) and a bias of -3.5 mg C m^{-3}, equivalent to 17% of the observed

485 mean. Model estimates and SEAMAP measurements also compare well with total

486 mesozooplankton biomass measurements (0.2-5 mm) collected in the oligotrophic region during

487 the process study cruises (Model: 5.55 ± 2.87 mg C m^{-3} vs. Cruise: 4.33 ± 2.28 mg C m^{-3}).

488 Although seasonal cycles in the oligotrophic and shelf regions could not be derived from the

489 SEAMAP dataset given the significant differences in sampling locations over the course of a year,

490 we investigated model-data mismatches for each month. The model closely matches or slightly

491 underestimates mesozooplankton biomass for most of the year, with the exception of January, May

492 and August (**Fig. 3A**). The largest model-data mismatch occurs during March, June, July and

493 December, when the model underestimates mesozooplankton biomass by approximately 35%.

494 Unlike surface Chl, the total mesozooplankton biomass (i.e. depth-integrated) seasonality is

495 similar in both regions of the GoM. In the oligotrophic region, the annual biomass minimum

496 (maximum) occurs at the beginning of January (middle of May), while in the shelf region, the

497 annual minimum (maximum) occurs in late December (end of May) (**Table 1**).

498
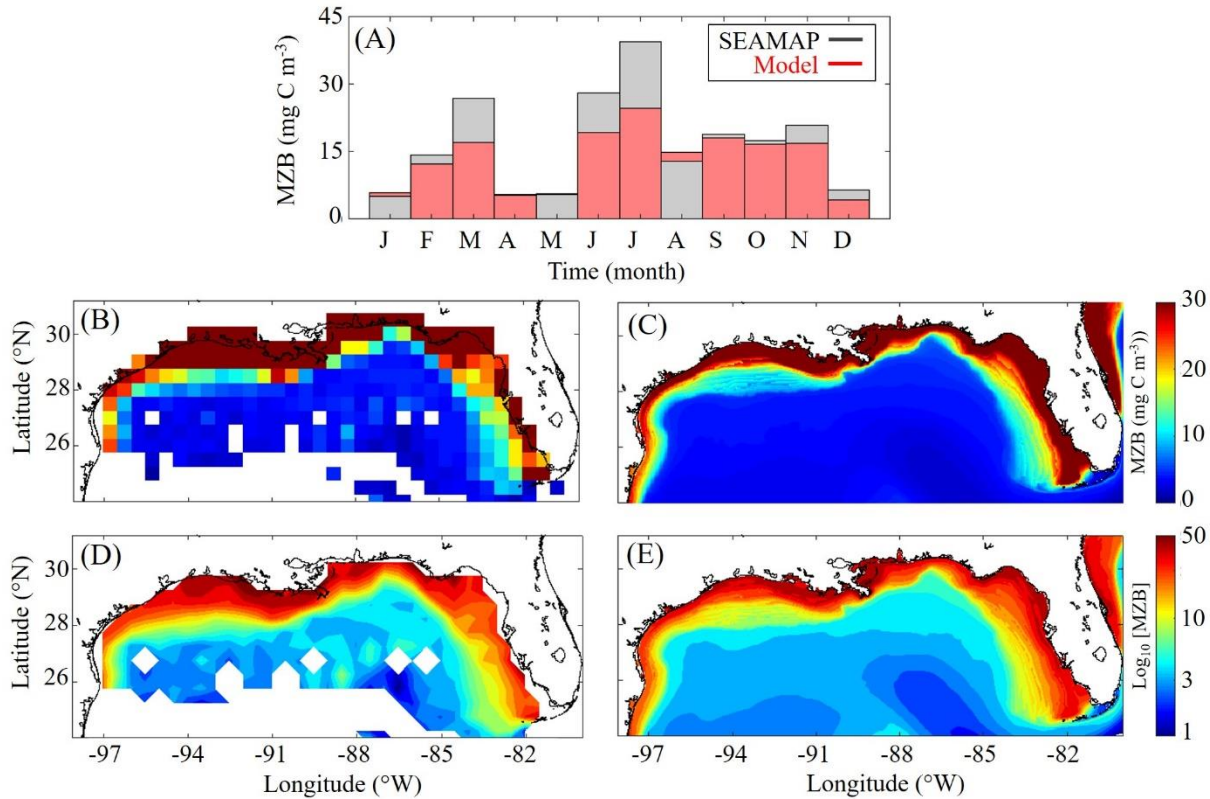
Figure 3 (A-E): Comparison of climatological depth-averaged (0–200 m) mesozooplankton biomass (MZB, mg C m^{-3}) between SEAMAP observations (B&D) and model (C&E). Monthly average MZB in SEAMAP observations (black) and model (red) (A) (monthly variability is not representative of MZB seasonality because sampling locations change between months). MZB climatology computed from SEAMAP plankton tows (B) and the corresponding log$_{10}$ field (D). MZB climatology computed from daily averages over the entire model simulation (1993-2012) (C) and the corresponding log$_{10}$ field (E).

3.3 Chlorophyll and nitrate profile model-data comparisons

To validate the vertical structure of the simulated ecosystem, we utilized observed profiles of fluorescence, Chl, and nitrate. When simulated DCM depths were compared to all 2,435 SEAMAP fluorescence profiles, we find a statistically significant correlation ($\rho = 0.59$, $p < 0.01$) with the observed maximum fluorescence depth. The maximum fluorescence depth ranged from the surface to 143 m while model values show a similar variability ranging from the surface to 163 m (**Fig. 4A**). In the oligotrophic region, the model overestimates the DCM depth (Model: 95 ± 20 m vs. SEAMAP: 80 ± 25 m) and has a ρ value of 0.38 ($p < 0.01$) with a bias of 15 m, equivalent

514   to 19% of the observed mean. In the shelf region, the model also overestimates DCM depth

515   (Model: 63 ± 26 m vs. SEAMAP: 53 ± 23 m) and has a ρ value of 0.49 (p < 0.01) with a bias of

516   10 m, equivalent to 19% of the observed mean.

517   In contrast, the model slightly underestimated the DCM depth when compared to calibrated

518   fluorescence profiles collected during the process cruises (Model: 100 ± 18 m vs. Observed: $107\pm$

519   21 m) (**Fig. 4B**). In terms of magnitude, the model overestimates DCM Chl (Model: 0.74 ± 0.35

520   mg Chl m^{-3} vs. Observed: 0.38 ± 0.13 mg Chl m^{-3}), although most of the observations fall within

521   one standard deviation of the model average. Despite this model-data mismatch, simulated nitrate

522   profiles closely match profiles from the World Ocean Database (WOD). In both model and

523   observations, the mean nitracline occurred at approximately 75 m (**Fig. 4C**). On average, model

524   nitrate tended to be lower at the surface and higher at depth relative to observations. Above the

525   nitracline, model nitrate was 0.071 ± 0.39 mmol N m^{-3} while observed nitrate was 0.55 ± 1.29

526   mmol N m^{-3}. Below 200 m, model and data show better agreement, with deep nitrate in the model

527   of 24.92 ± 3.28 mmol N m^{-3} compared to 23.55 ± 5.21 mmol N m^{-3} in WOD profiles.
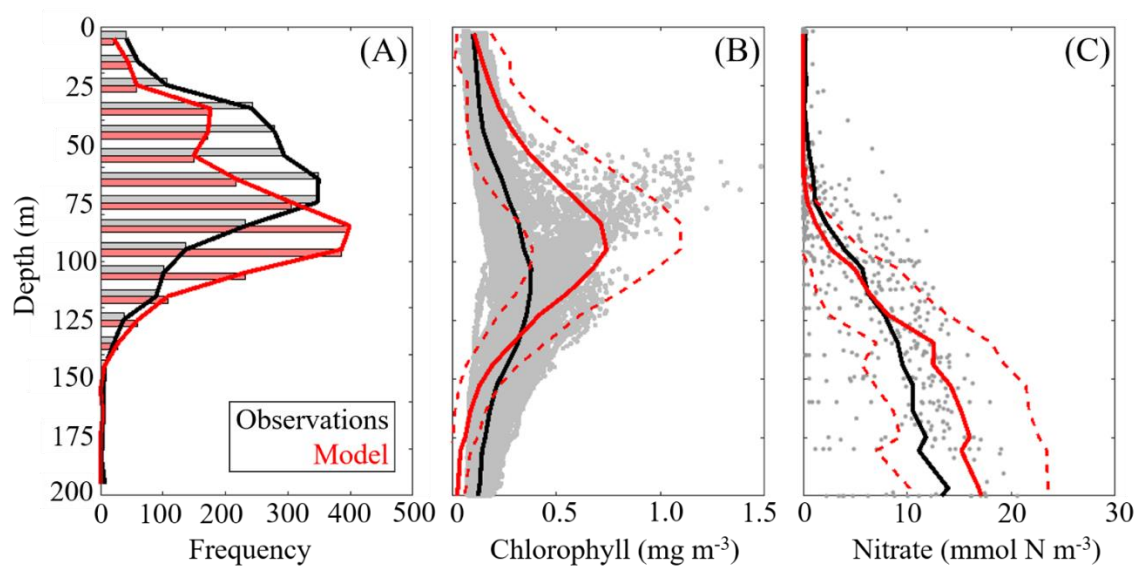
528

529   **Figure 4 (A-C):** Model-data comparisons in the vertical distribution of chlorophyll (A&B) and

530   nitrate (C). Comparison between maximum fluorescence depths observed in SEAMAP profiles

531   and simulated maximum chlorophyll depths (m) (A). Comparison between in situ chlorophyll

532   samples collected during May, 2017 and 2018 process study cruises and simulated chlorophyll

533   concentrations (mg m^{-3}) (B). Grey dots represent cruise sample values and red dashed line denotes

534   1 standard deviation away from the model average. Comparison between nitrate profiles obtained
535   from World Ocean Database (WOD) and simulated nitrate (mmol N m^{-3}) (C). Gey dots represent
536   WOD sample values and red dashed line denotes 1 standard deviation away from the model
537   average.

538   DCM depth was evaluated using un-calibrated fluorescence profiles obtained during SEAMAP
539   cruises. Chlorophyll profiles were collected during the May 2017 and 2018 Lagrangian process
540   cruises. For comparisons, the model and data were sampled at corresponding locations and time
541   of the year for all simulated years. Nitrate values from World Ocean Database that overlapped with
542   the simulation period and were located in the oligotrophic GoM (>1000 m) were used for model-
543   data comparisons.

3.4   Size fractionated mesozooplankton biomass and grazing model-data comparisons

545   To further constrain the phytoplankton and zooplankton community simulated by NEMURO-
546   GoM, we utilized in situ measurements collected during the process study cruises. First, we
547   compared the relative proportions of LZ and PZ biomass to four discrete size classes measured at
548   sea **(Fig. 5A, C)**. In both model and observations, we find nearly identical size distributions
549   assuming that LZ approximates the smallest two size classes of mesozooplankton sampled ("small
550   mesozooplankton", 0.2-1.0-mm) and PZ approximates the largest two size classes ("large
551   mesozooplankton", 1.0-5.0 mm). In the field data, small mesozooplankton biomass varied from
552   33 to 46 % (median = 40%, at 95% C.I.), while model estimates of LZ biomass vary from 31 to
553   46% (median = 40%). Large mesozooplankton biomass in the field data varied from 54 to 67%
554   (median = 60%), while model estimates of PZ biomass vary from 54 to 69% (median = 60%).
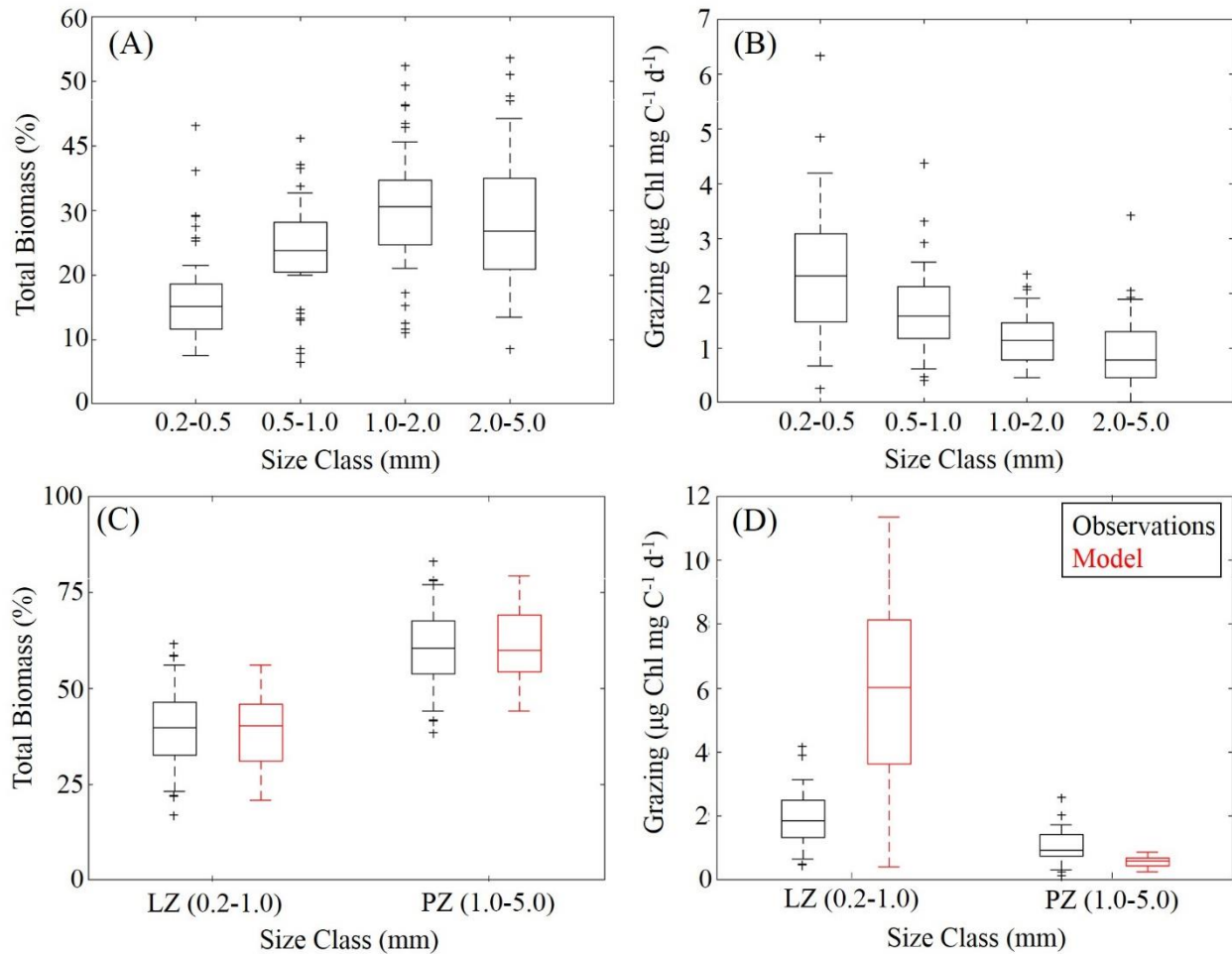
Figure 5 (A-D): Mesozooplankton size-fractioned biomass (A&C) and grazing rates (C&D) in field measurements (black) and model estimates (red). Mesozooplankton size-fractioned biomass measured during May 2017 and May 2018 process study cruises (A) along with corresponding measured grazing rates (B). Comparisons of model estimated mesozooplankton biomass to aggregated (size class 1-2, 3-4) field measurements (C). Comparisons of model estimated specific mesozooplankton grazing rates to aggregated (size class 1-2, 3-4) field measurements (D). Whiskers extend to 95% confidence interval. Outliers for model estimates are not shown.

Mesozooplankton specific grazing rates measured during the process study cruises were also used to validate the simulated mesozooplankton community. Field measurements showed that specific grazing rates (μg Chl mg C^{-1} d^{-1}), decreased consistently with increasing mesozooplankton size-class (**Fig. 5B**). For model-data comparisons, we computed grazing on LP by LZ and PZ at each depth. Grazing terms were converted into units of Chl using the model estimated C:Chl ratio for

568 LP before being depth-integrated to the corresponding net tow depth and normalized to simulated

569 depth-integrated LZ and PZ biomasses. We find that model mesozooplankton grazing estimates

570 capture the general trend of decreased specific grazing rates with increasing mesozooplankton size

571 (**Fig. 5D**). However, the model overestimates grazing by small mesozooplankton while

572 underestimating grazing by large mesozooplankton. In the field data, small mesozooplankton

573 grazing ranges from 1.34 to 2.51 µg Chl mg C^{-1} d^{-1} (median = 1.85) while model estimates of LZ

574 grazing rates vary from 3.64 to 8.14 µg Chl mg C^{-1} d^{-1} (median = 6.01). Field measurements of

575 large mesozooplankton grazing range from 0.76 to 1.44 µg Chl mg C^{-1} d^{-1} (median = 0.94), while

576 model estimates of PZ grazing vary from 0.44 to 0.70 µg Chl mg C^{-1} d^{-1} (median = 0.58). In terms

577 of total grazing, the model average is also considerably higher (2.99 $\pm$ 2.20 µg Chl mg C^{-1} d^{-1})

578 relative to field measurements (1.38 $\pm$ 0.59 µg Chl mg C^{-1} d^{-1}) (see Discussion).

579 **3.5   Phytoplankton growth and microzooplankon grazing model-data comparisons**

580 Measurements of specific phytoplankton growth rates, phytoplankton mortality due to

581 microzooplankon grazing, and net primary production (NPP) were used to evaluate protistan

582 dynamics in the model. We find the model underestimates phytoplankton growth and

583 microzooplankton grazing while overestimating NPP (**Fig. 6A, B**). Phytoplankton specific growth

584 rates from dilution experiments range from 0.50 to 0.66 d^{-1} (median = 0.55 d^{-1}) while model

585 estimates of phytoplankton (SP+LP) specific growth rates vary from 0.13 to 0.27 d^{-1} (median =

586 0.21 d^{-1}). In terms of microzooplankton grazing rates, field data range from 0.19 to 0.55 d^{-1} (median

587 = 0.39 d^{-1}) while model estimates of SZ vary from 0.10 to 0.21 d^{-1} (median = 0.16 d^{-1}). NPP

588 estimates show better agreement with observations with rates from 276 to 360 mg C m^{-2} d^{-1}

589 (median = 321 mg C m^{-2} d^{-1}) in field data while model estimates vary from 190 to 741 mg C m^{-2}

590 d^{-1} (median = 431 mg C m^{-2} d^{-1}).

591 Although the model underestimates phytoplankton growth and microzooplankton grazing rates,

592 the relative proportion of NPP consumed by protists in the model (67 - 85%; median = 76%)

593 compares reasonably well to field measurements (55 - 92%; median = 72%) (**Fig. 6C**). Notably,

594 the model average proportion of phytoplankton production consumed by protists closely matches

595 the mean for all tropical waters reported by Calbet & Landry (2004). When phytoplankton

596 mortality due to mesozooplankton grazing was evaluated in the model at cruise sample locations

597 we find mesozooplankton grazing accounts for 13 ± 8 %, which also closely agrees with the global

598 average (Calbet et al., 2001).
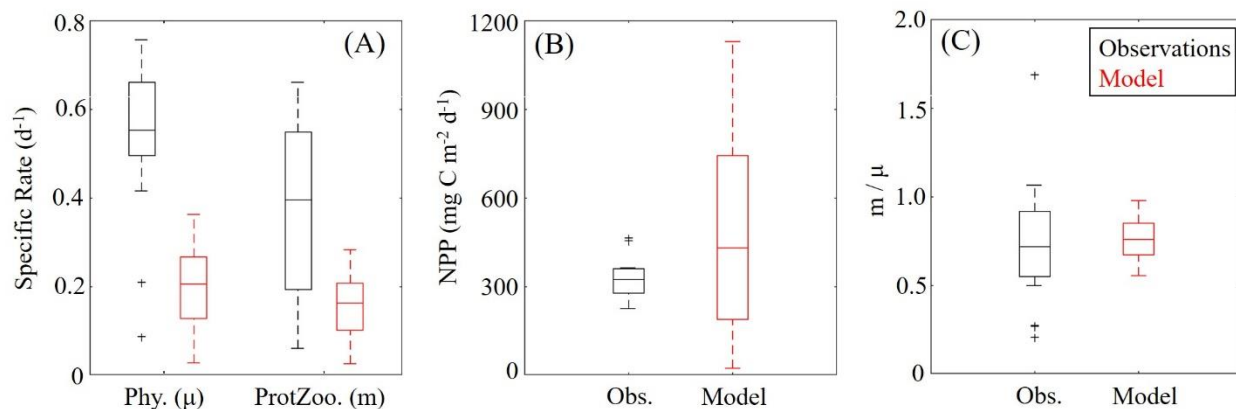
599

600 **Figure 6 (A-C):** Specific phytoplankton growth (μ, d^{-1}) and microzooplankon grazing (m, d^{-1})

601 between model (red) and field data (black) (A). Depth-integrated net primary production (mg C

602 m^{-2} d^{-1}) (B). The fraction of phytoplankton growth that is grazed by protists in the model and field

603 data (C). Whiskers extend to the 95% confidence intervals. Outliers for model estimates are not

604 shown.

605 ### 3.6   Simulated mesozooplankton diet

606 After model tuning and validation, we utilized NEMURO-GoM to investigate spatiotemporal

607 variability in diet and secondary production of the GoM mesozooplankton community. First, we

608 examined the trophic level of LZ and PZ in the model, which provides a measure of their

609 cumulative diet. Trophic level is calculated by computing the dietary contributions of each prey in

610 LZ (i.e. LP and SZ) and PZ diets (i.e. LP, SZ, and LZ), assuming that the trophic level of LP = 1

611 and SZ = 2. In the oligotrophic region, both LP and SZ contribute approximately 50% to LZ diet,

612 as indicated by a mean trophic level near 2.5 (2.54 ± 0.02) for LZ (**Fig. 7A**). In the same region,

613 PZ have a trophic level of 2.78 ± 0.04 indicating a higher contribution of zooplankton to their diet

614 (i.e. SZ and/or LZ) (**Fig. 7B**). In the shelf region, LZ are more herbivorous, as indicated by a

615 decrease in trophic level to 2.31 ± 0.01, while PZ are more carnivorous, as indicated by an increase

616 in trophic level to 2.90 ± 0.04.

617 Despite little evidence for LZ diets dominated by zooplankton in the annual average (in contrast

618 to PZ, which often have a trophic level ~3), we commonly find regions in instantaneous fields

619   during both winter and summer conditions where SZ are the dominant prey source for LZ (**Fig.**
620   **7C, E**). These regions, typically in the Loop Current or Loop Current Eddies (LCEs), highlight the
621   episodic importance of heterotrophic protists as prey sources for small mesozooplankton in the
622   GoM. High proportions of SZ in LZ diets can be attributed to the competitive advantage of SP
623   over LP in extremely low nutrient environments such as in the Loop Current, resulting in high
624   abundances of SP and their predators (SZ) relative to LP. Instantaneous fields also reveal that
625   phytoplankton can be important prey for PZ as well, particularly during summer, as indicated by
626   trophic levels of around 2.5 in the western GoM (**Fig. 7F**). In addition to strong variability in
627   trophic positions, there are also regions in the oligotrophic GoM, most clearly in the centers of
628   LCEs during summer, where the model predicts no feeding by mesozooplankton (**Fig. 8E**). The
629   convergent anti-cyclonic circulation of LCEs is typically associated with low phytoplankton
630   biomass, which at times may fall near or below feeding thresholds in the NEMURO grazing
631   formulation. This formulation is intended to simulate suppression of feeding activity for
632   zooplankton at mean prey densities that cannot support the energy expended while searching for
633   prey.

634   To investigate which prey contributes most to LZ and PZ diets, we computed each prey source
635   term for both LZ and PZ at each grid cell (**Fig. 8**). As one would expect, the dominant prey for LZ
636   and PZ align closely with spatial variability in their respective trophic positions. For LZ diet,
637   herbivory dominates throughout the GoM, except for the Loop Current (**Fig. 8A**). LP contribution
638   to LZ diet is highest on the shelf, where LP biomass is also high due to the competitive advantage
639   of LP over SP in high nutrient conditions. In contrast, PZ diet varies with the relative availability
640   of SZ and LZ prey. In the oligotrophic region, PZ feed mainly on SZ (heterotrophic protists)
641   because LZ biomass is relatively low. On the shelf, they consume primarily LZ (**Fig. 8D**). Despite
642   the significant change in diet between the shelf and oligotrophic regions, PZ trophic positions
643   remain fairly consistent (**Fig. 7D**). This is due to the fact that SZ in the oligotrophic region and LZ
644   in the shelf region both feed predominantly on phytoplankton and hence occupy similar trophic
645   levels. In the instantaneous fields for winter (**Fig. 8B, E**) and summer (**Fig. 8C, F**), the dominant
646   prey for both LZ and PZ show substantial mesoscale variability, indicating that oceanographic
647   features such as fronts and eddies influence not only biomass but also zooplankton ecological roles
648   (see Discussion).

649
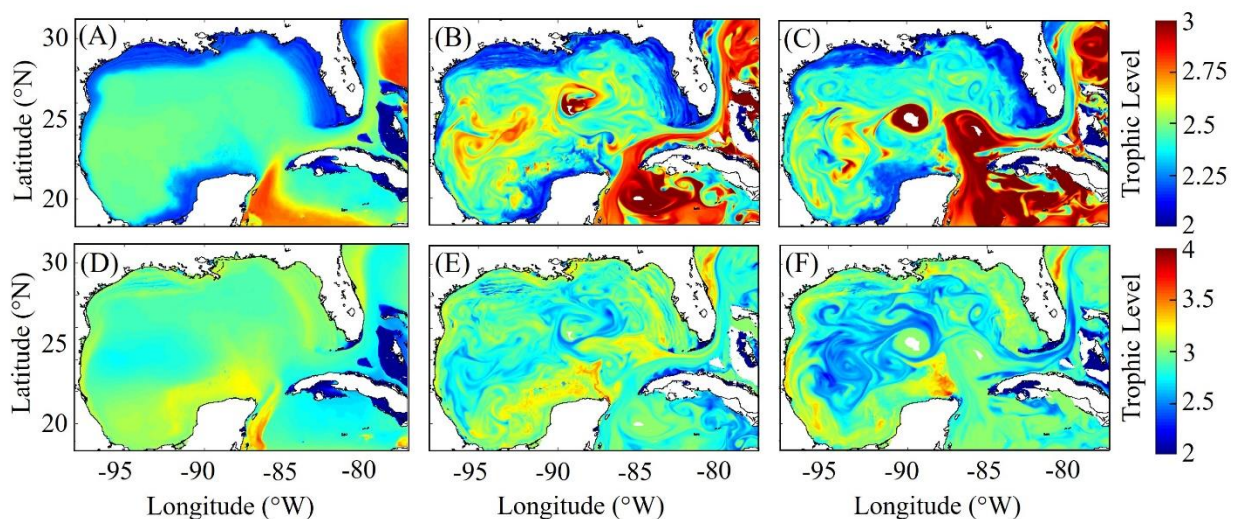
Figure 7 (A-F): Trophic levels of simulated large zooplankton (LZ, top) and predatory zooplankton (PZ, bottom). Annual-averaged trophic positions of LZ (A) and PZ (D). Instantaneous model field of trophic positions during winter conditions for LZ (B) and PZ (E) on 4 February 2012. Instantaneous model field of trophic positions during summer conditions for LZ (C) and PZ (F) on 2 August 2011.

655
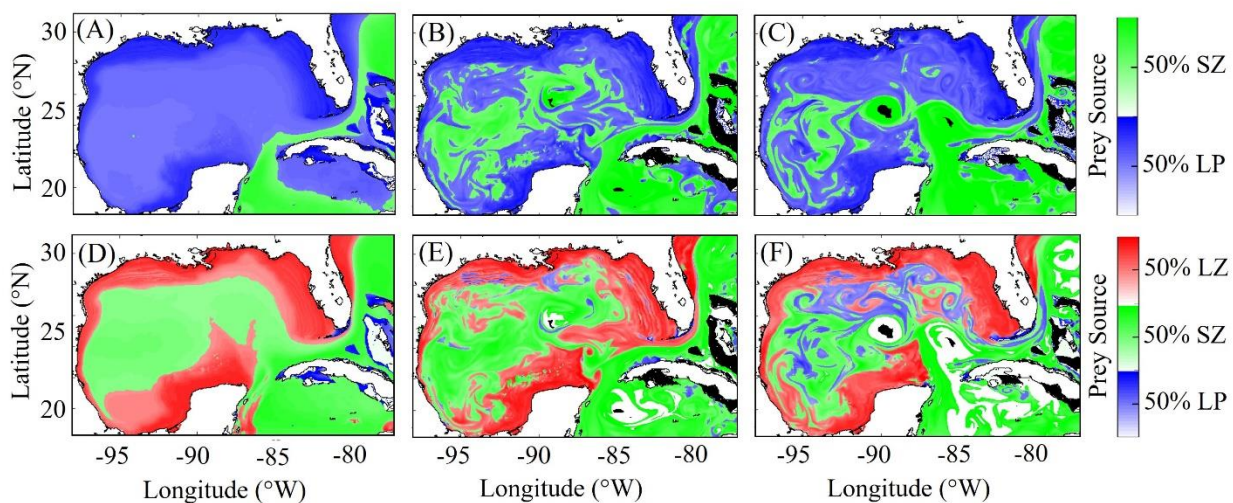
Figure 8 (A-F): Dominant prey source for simulated large zooplankton (LZ, top) and predatory zooplankton (PZ, bottom). Annual-averaged diet contributions for LZ (A) and PZ (D). Instantaneous model field of zooplankton diet during winter conditions for LZ (B) and PZ (E) on 4 February 2012. Instantaneous model field of zooplankton diet during summer conditions for LZ (C) and PZ (F) on 2 August 2011.

3.7 Simulated mesozooplankton secondary production

To our knowledge, regional secondary production for the GoM has not been quantified previously. Based on our model, secondary production due to mesozooplankton averages 66 ± 8 x 10^6 kg C yr^{-1}, and ranged from a minimum of 51 x 10^6 kg C (in 1999) to a maximum of 82 x 10^6 kg C (in 2011). In the oligotrophic region, LZ secondary production averages 35 ± 5 mg C m^{-2} d^{-1} while PZ secondary production is 11 ± 2 mg C m^{-2} d^{-1} (**Fig. 9**). The annual secondary production minimum develops at the end of December while the annual maximum occurs at the beginning of June (**Table 1**). In this region, mesozooplankton secondary production is 14 ± 2 x 10^6 kg C yr^{-1}, equivalent to 6% of NPP. On the shelf, secondary production is about 4-fold higher, with LZ production of 146 ± 17 mg C m^{-2} d^{-1} and PZ production of 42 ± 5 mg C m^{-2} d^{-1}. Here, the annual minimum also occurs at the end of December while the maximum occurs later at the end of July (**Table 1**). On the shelf, secondary production constitutes a higher proportion of NPP (13%) and averages 51 ± 6 x 10^6 kg C yr^{-1}.

In addition to differences in total secondary production, significant differences were found in the mesozooplankton community response to changes in total phytoplankton biomass on the shelf and in the oligotrophic region. On the shelf, the average ratio between LZ and PZ secondary production is 3.51 and remains almost constant with increasing phytoplankton biomass ($\rho = 0.13$, $p < 0.01$). Although we find a similar average value in the oligotrophic region (3.14), ratios are more variable and strongly dependent on phytoplankton biomass ($\rho = 0.52$, $p < 0.01$). Ratios of LZ to PZ secondary production reached values of ~2.5 in the lowest phytoplankton biomass regions of the open ocean GoM and increased to ~4.0 during times and places where local phytoplankton biomass was high. These differences likely stem from the longer turnover times of PZ, which make them less sensitive to variability in bottom-up drivers and allows them to have a proportionally greater role in oligotrophic settings.

As witnessed in the instantaneous fields of diet and secondary production, mesoscale eddies are common features in the GoM and hence important to quantify for regional zooplankton dynamics. To investigate secondary production inside cyclonic and anticyclonic eddies we implement the TOEddies eddy detection algorithm (Laxenaire et al., 2018) which uses surface velocities along closed contours of sea surface height (SSH) for detection of mesoscale eddies (Chaigneau et al., 2011; Laxenaire et al., 2019; Pegliasco et al., 2015). Grid cells located inside

691 each eddy are defined within the SSH contour associated with the maximum mean surface velocity
692 (interior grid cells). Grid cells located between the outer most closed contour and within 1.5 radius
693 of the eddy center and not within another eddy were used to define background conditions outside
694 of eddies (exterior grid cells). Only eddies with areas larger than an equivalent circular diameter
695 of 100 km and not within the Loop Current were considered in the analysis. On average, 3.78
696 cyclonic and 3.33 anticyclonic eddies were identified in each daily velocity field.

697

698 In the model cyclonic eddies were associated with 10% higher secondary production relative to
699 exterior grid cells and the ratio of secondary production in interior cells to exterior cells ranged
700 from 0.4 to 3.37 (95% CI). In contrast, secondary production was substantially lower inside
701 anticyclonic eddies accounting for only 46% of the average secondary production in exterior cells
702 (0.03 - 1.87 (95% CI)). In addition to their convergent nature that dampens nutrient input, lower
703 rates of secondary production in anticyclonic eddies can likely be attributed to the presence of
704 highly oligotrophic Loop Current water trapped within large anticyclonic LCEs.
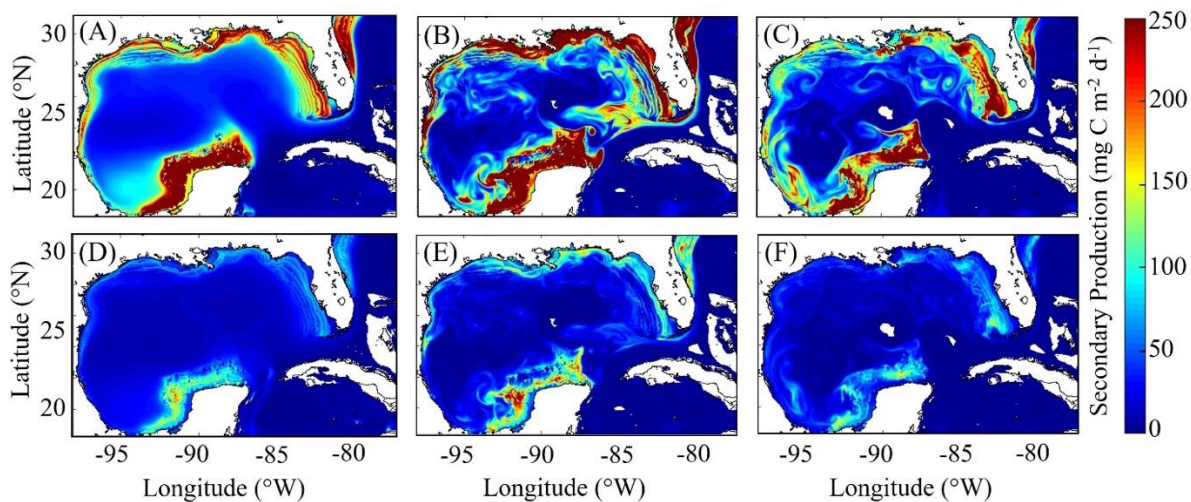
705

706 **Figure 9 (A-F):** Vertically integrated secondary production (mg C m^{-2} d^{-1}) of simulated large
707 zooplankton (LZ, top) and predatory zooplankton (PZ, bottom). Annual-averaged secondary
708 production for LZ (A) and PZ (D). Instantaneous model field of secondary production during
709 winter conditions for LZ (B) and PZ (E) on 4 February 2012. Instantaneous model field of
710 secondary production during summer conditions for LZ (C) and PZ (F) on 2 August 2011.

Table1: Average seasonal minimum and maximum values in the model (1993-2012) and the day of year in which they occur for surface chlorophyll (mg m^{-3}), depth-integrated estimates of phytoplankton biomass (mg C m^{-2}), net primary production (mg C m^{-2} d^{-1}), mesozooplankton biomass (mg C m^{-2}), and mesozooplankton secondary production (mg C m^{-2} d^{-1}) calculated by spatially averaging daily fields over the oligotrophic region (grid cells with bottom depths $\geq$1000m) and shelf region (grid cells with bottom depths < 1000 m). Day of year values are in the format "day/month $\pm$ days."

	Daily Field Value		Day of Year	
Diagnostic (Oligotrophic)	Annual Min.	Annual Max.	Day of Min.	Day of Max.
Surface Chlorophyll	0.09 $\pm$ 0.005	0.27 $\pm$ 0.06	9/9 $\pm$ 23	1/29 $\pm$ 13
Phytoplankton Biomass	2300 $\pm$ 130	3600 $\pm$ 140	12/26 $\pm$ 7	4/29 $\pm$ 17
Net Primary Production	290 $\pm$ 70	1000 $\pm$ 120	12/31 $\pm$ 12	7/6 $\pm$ 27
Mesozooplankton Biomass	1000 $\pm$ 40	1400 $\pm$ 90	1/1 $\pm$ 4	5/19 $\pm$ 18
Secondary Production	18 $\pm$ 4	68 $\pm$ 10	12/31 $\pm$ 10	6/4 $\pm$ 15
Diagnostic (Shelf)	Annual Min.	Annual Max.	Day of Min.	Day of Max.
Surface Chlorophyll	1.96 $\pm$ 0.15	3.00 $\pm$ 0.30	2/8 $\pm$ 37	7/31 $\pm$ 58
Phytoplankton Biomass	3200 $\pm$ 290	5200 $\pm$ 440	1/1 $\pm$ 9	7/18 $\pm$ 11
Net Primary Production	750 $\pm$ 120	2000 $\pm$ 220	12/31 $\pm$ 8	7/21 $\pm$ 14
Mesozooplankton Biomass	670 $\pm$ 70	1100 $\pm$ 90	12/29 $\pm$ 7	5/23 $\pm$ 25
Secondary Production	94 $\pm$ 17	270 $\pm$ 28	12/31 $\pm$ 6	7/20 $\pm$ 16

4.0   Discussion

Many parameters in biogeochemical models are poorly constrained by observations and laboratory studies and/or highly variable in the environment. The numbers and uncertainties around these parameters allow PBMs with varying degrees of tuning to reproduce a single ecosystem attribute (e.g., surface Chl) even if multiple processes are inaccurately represented (Anderson, 2005; Franks, 2009). Once validated, one of the main values of coupling physical and biogeochemical models (i.e. PBMs) is their utility for making inferences about portions of the lower trophic level that are under sampled and/or difficult to measure in the field. If PBMs are to be utilized to explain variability rather than simply fit an observational dataset, multiple ecosystem attributes, must be validated and the underlying model structure and assumptions critically evaluated. In the section

729 below, we further justify changes to model structure by evaluating the underlying assumptions in

730 default NEMURO and discuss model-data mismatch before drawing conclusions about the GoM

731 zooplankton community and the implications of its dynamics for higher trophic levels.

4.1 Justification for NEMURO modifications

733 The phytoplankton community in the North Pacific (NP) domain where NEMURO was originally

734 designed is largely composed of nanoplankton (original SP) and microplankton (original LP). By

735 default, SP is assumed to represent coccolithophores and autotrophic nanoflagellates, which can

736 be important prey of copepods and other mesozooplankton in temperate and subpolar regions

737 (Kishi et al., 2007). However, in tropical regions such as the GoM, smaller picophytoplankton taxa

738 typically dominate, particularly in highly oligotrophic regions. Common picophytoplankton of the

739 GoM include cyanobacteria and picoeukaryotes, which are too small for most mesozooplankton

740 to feed on. Hence, the SP to LZ grazing pathway was removed in our model. We found that

741 removal of this grazing pathway allowed the model to simulate a more realistic phytoplankton

742 community on the shelf region. Despite intuition, SP largely dominated the shelf region in the

743 model when LZ were allowed to graze on SP. After closer inspection, we found that grazing of SP

744 sustained LZ biomass on the shelf to levels where top-down pressure constrained LP standing

745 stocks. This prevented large blooms of LP, leading to a competitive advantage for SP even in

746 highly eutrophic conditions (the Mississippi river delta), which was observed for a wide range of

747 LP maximum growth rates, LP half-saturation constants, and LZ/PZ grazing rates. Thus, removal

748 of the SP to LZ grazing pathway added ecological realism and improved the model solution.

749 During the model tuning process (outlined in the supplemental), we also found that, despite a wide

750 range of tested parameter sets, the model was unable to simulate mesozooplankton biomass low

751 enough to match SEAMAP observations in the oligotrophic region. Even with unrealistically low

752 phytoplankton biomass, equivalent to approximately 50% of surface Chl observed in SeaWIFS

753 images, the model overestimated mesozooplankton biomass. To achieve realistic levels of

754 mesozooplankton biomass in the oligotrophic region, default LZ and PZ mortality parameter

755 values needed to be increased by an order of magnitude. However, this produced unrealistically

756 high loss rates on the shelf region, leading to mesozooplankton biomass estimates that were

757 substantially lower than SEAMAP shelf observations. Implementation of linear mortality on all

758 biological state variables (except PZ) resolved this issue by providing the model with a greater

759 dynamic range. In NEMURO, and other biogeochemical models, quadratic mortality is often used
760 to increase model stability and/or is mechanistically justified as representing the impact of
761 unmodeled predators that co-vary in abundance with prey (Gentleman and Neuheimer, 2008;
762 Steele and Henderson, 1992). However, grazing losses of all state variables (except PZ), are
763 already explicitly modeled in NEMURO by default. Hence, removal of quadratic mortality also
764 added ecological realism and improved the model solution. Quadratic mortality was retained for
765 PZ to account for the implicit predation pressure of un-modeled predators (e.g. planktivorous fish).

766 ## 4.2 Model-data mismatch

767 ### 4.2.1 Surface chlorophyll discrepancies

768 Within our model-data comparisons of surface Chl we find that NEMURO-GoM reproduces
769 important patterns in both the oligotrophic and shelf region. The latter of which, apart from the
770 northern shelf, has not been well resolved by previous PBMs (e.g., Gomez et al., 2018; Xue et al.,
771 2013). The absence of a shelf Chl signature may, in some cases, be overly attributed to bias in
772 satellite measurement due to high concentrations of colored dissolved organic matter (CDOM).
773 While a clear shelf signature is well resolved in NEMURO-GoM, the model-data mismatch is
774 greater on the shelf compared to oligotrophic regions. This is an expected result considering that
775 the model incorporates climatological river forcing while actual variability is much more complex.
776 Furthermore, the absence of CDOM in the model likely contributes to the overestimation of
777 phytoplankton biomass on the shelf.

778 In future studies, the inclusion of daily nutrient data like that produced for the Mississippi River
779 by USGS starting in 2011 is needed for PBMs to better resolve variability on the shelf. Including
780 benthic processes, such as denitrification (Fennel et al., 2006), may also reduce model-data
781 mismatch in shelf regions. Implementing more realistic light attenuation (e.g. wavelength-specific
782 light attenuation or inclusion of CDOM) could further improve estimates of phytoplankton
783 biomass on the shelf as primary production can be sensitive to different light attenuation
784 formulations (Anderson et al., 2015). In our model, it was difficult to simulate deep DCMs in the
785 oligotrophic GoM while also simulating DCMs on the shelf that were shallow enough to maintain
786 high nitrate. This may reflect the need for more realistic light attenuation in the model.

787 Quantifying uncertainty in C:Chl ratios is also an important task moving forward as future PBMs
788 will likely continue to depend heavily on satellite Chl for the bulk of model validation. To correctly
789 parameterize C:Chl ratios more in situ samples are needed that resolve changes in phytoplankton
790 light harvesting pigments along gradients from coastal to oligotrophic regions and from the surface
791 to the DCM. Without these observations, it is difficult to gauge mismatches between model and
792 satellite ocean color products (e.g. discrepancies on the Campeche Bank in our model) or in situ
793 profiles of Chl. In addition to validation, these measurements are needed to avoid erroneous model
794 tuning. For instance, a model that exhibits significant mismatch with respect to surface Chl may
795 in fact accurately estimate carbon based phytoplankton biomass while using unrealistic C:Chl
796 ratios. One could arrive at incorrect conclusions about regional ecosystem dynamics as a result of
797 modifying model parameters or structure in an effort to better fit Chl observations. Given the
798 importance of C:Chl ratios in PBMs, future studies should quantify uncertainty in modeled Chl
799 through sensitivity experiments focused on C:Chl model parameters and formulation, with explicit
800 comparison to direct field measurements of phytoplankton C:Chl.

801 In our model, the most noticeable surface Chl model-data mismatch occurs on the southern GoM
802 shelf (Campeche Bank), where the model consistently overestimates surface Chl. This bias was
803 also notable in the GoM PBM implemented by Damien et al. (2018), particularly in winter. We
804 believe this discrepancy is driven by a combination of errors involving overestimation of shelf
805 mixing by the hydrodynamic model, entrainment of high Chl water (given the overestimated DCM
806 magnitude in the model), or errors in the open boundary conditions which result in an
807 overestimation of upwelled nutrients/biomass near the Yucatan Peninsula that are transported
808 westward by shelf currents. We found that the Campeche Bank model-data mismatch was reduced
809 when open boundary conditions included nitracline depths of greater than 100 m. This may reflect
810 realistic in situ conditions considering that Caribbean water entering the GoM is highly
811 oligotrophic. During our process cruises, nitrate was often undetectable above 100 m in samples
812 collected near the Loop Current (A. Knapp, pers. comm.).

813 Although modifying the boundary conditions may be justified, deepening the nitracline at the
814 boundaries made it increasingly difficult to sustain realistic surface phytoplankton biomass in the
815 oligotrophic GoM. This may point to the importance of nitrogen fixing cyanobacteria, which
816 provide an alternative source of new nitrogen (other than upwelling and mixing) that could be

817 supporting phytoplankton at the surface given the strong stratification and deep nitraclines in the

818 GoM. In the process of model tuning, we noticed that increasing the DON pool by increasing the

819 PON to DON decomposition rate was necessary to maintain both relatively deep nitraclines and

820 realistic surface Chl by providing a slow leeching of ammonium near the surface through bacterial

821 communities. The need for this slow production of ammonium in surface layers may compensate

822 for nitrogen fixation, which is not included in NEMURO (Holl et al., 2007; Mulholland et al.,

823 2006). In future studies, including diazotrophs as a separate phytoplankton functional type would

824 be essential for evaluating the importance of nitrogen fixation in the GoM.

825 Despite the model-data mismatch on the Campeche Bank, this discrepancy appears to have little

826 impact on the rest of the GoM. However, the model overestimates surface Chl in the southwestern

827 GoM, which can likely be attributed to entrainment of high Chl water originating from the

828 Campeche Bank. Locally, the ecological impact is likely more significant. Higher phytoplankton

829 biomass would be expected to support higher mesozooplankton grazing rates and secondary

830 production. Indeed, some of the highest model rates of secondary production occur on the

831 Campeche Bank. Hence, the surface Chl model-data mismatch may lead to an overestimation of

832 secondary production for this region.

4.2.2 Deep chlorophyll maximum discrepancies

834 Since most PBMs focus on validating against satellite derived surface chlorophyll, the dynamics

835 of the DCM is often insufficiently investigated. Consequently, many models predict DCM depths

836 that are far too shallow. Identifying this issue in the literature proved to be difficult because most

837 studies do not provide profiles of simulated Chl (an exception is the recent GoM PBM by Damien

838 et al. (2018)). We note that DCM depths in the DIAZO model (Stukel et al., 2014) were often quite

839 shallow or completely nonexistent in the portion of the domain that included the oligotrophic GoM

840 region. Underestimates of DCM depth in the unmodified COBALT biogeochemical model has

841 also been identified (Moeller et al., 2019). In our investigation of the GoM PBM implemented by

842 Gomez et al. (2018), we found that DCMs in the oligotrophic region were commonly shallow and

843 weak. In the default NEMURO simulation, DCM depths in the oligotrophic region were typically

844 at a depth of 25 m, which is much shallower than observed (SEAMAP: 80 ± 25 m, Process cruises:

845 107 ± 21 m). While this issue may seem insignificant, particularly if a study is focused on mixed-

846 layer dynamics, accurate placement of the DCM can have profound impacts on PBM behaviors,

847 because the DCM is typically co-located with the nitracline. Unrealistically shallow DCMs and

848 nitraclines permit unrealistically high nitrate fluxes into the surface layer following mixing events;

849 thus, validating the DCM in PBMs is critical.

850 For these reasons, we devoted substantial effort to tuning phytoplankton dynamics in the DCM.

851 Modifications to α (the slope of the photosynthesis-irradiance curve) and attenuation coefficients

852 allowed the model to estimate deeper more realistic DCM depths. Inclusion of a variable C:Chl

853 module was also implemented to better resolve the DCM. However, an additional issue was

854 present in the default NEMURO simulations, the NEMURO-GoM, and every simulation that we

855 attempted. In all simulations that formed DCMs, the location of the DCM was always co-located

856 with a maximum in phytoplankton specific growth rate, even though field measurements indicate

857 that phytoplankton growth rates and NPP are either relatively constant with depth or decline in the

858 DCM. This is not surprising, given the low photon flux at the base of the euphotic zone and the

859 energetic demands required to up-regulate cellular density of light harvesting pigments.

860 Additionally, our field measurements show that the DCM was not associated with a biomass

861 maximum (biomass was fairly constant with depth), suggesting that DCM formation in the GoM

862 is physiologically driven.

863 We believe this DCM dynamical issue was responsible, in part, for the underestimation of specific

864 phytoplankton growth and microzooplankon grazing rates by the model despite estimating higher

865 NPP (**Fig. 4D**). An underestimation of C:Chl ratios or overestimation of phytoplankton biomass

866 may also contribute to the model-data mismatch at the DCM. The ecological impact of this

867 mismatch is likely to be greatest in the model during the summer months when the mixed layer

868 depth is shallow and the DCM reaches its maximum depth. Elevated growth rates or biomass at

869 the DCM during this period could significantly decrease nitrate flux into the mixed layer causing

870 the model to underestimate near surface primary and secondary production.

871 Future PBM studies need to focus more effort on resolving ecological dynamics responsible for

872 the formation of the DCM. Errors originating from the hydrodynamic model or use of temporally

873 averaged velocity fields used in offline models may also contribute to model-data mismatch at the

874 DCM. Vertical mixing is particularly important to PBMs, but is often poorly validated in

875 hydrodynamic models. Greater coordination between physical modelers and biologists to constrain

876   vertical fluxes should be considered an important avenue for improving PBM simulations moving

877   forward.

4.2.3   Mesozooplankton grazing discrepancies

879   Novel to this study, model estimates of mesozooplankton biomass are shown to agree closely with

880   observations on the shelf and in the oligotrophic GoM. To our knowledge, this study includes the

881   first quasi-regional zooplankton biomass model validation in a PBM. Our model also provides the

882   first model-data comparisons of size-specific zooplankton biomass and grazing rates for the GoM.

883   Such comparisons provide valuable insights into the potential biases of traditional functional group

884   biogeochemical models pertaining to zooplankton dynamics (Everett et al., 2017). While

885   NEMURO-GoM shows broad agreement with zooplankton observations, some model-data

886   mismatch occurs, particularly for mesozooplankton grazing rates.

887   We identify three factors that may explain the model-data mismatch for mesozooplankton grazing

888   rates. The first and most obvious factor is the temporal sampling discrepancy as measurements

889   were collected outside our model simulation period. Model-data mismatch may also arise from

890   inaccuracies in the field measurements. During our process cruises, the zooplankton gut pigment

891   measurements were based solely on phaeopigment content due to phytodetrital aggregates and

892   *Trichodesmium* colonies found in our zooplankton net tows, which can lead to substantial

893   contamination. Thus, true mesozooplankton grazing rates were likely underestimated because

894   undegraded Chl can be abundant in the foreguts of mesozooplankton. Furthermore, the gut pigment

895   approach assumes that any group of mesozooplankton has a constant gut throughput time (as a

896   function of temperature), which is an oversimplification.

897   Uncertainties in model grazing formulations could also contribute to model-data mismatch

898   (Gentleman et al., 2003a; Sailley et al., 2015). Future in situ grazing measurements are needed to

899   enable an objective selection of grazing formulations and parameter values. In particular, field

900   studies that shed light on prey selectivity would be useful for parameterizing PBMs with multiple

901   mesozooplankton functional groups, such as NEMURO-GoM. Such studies are challenging,

902   however, because the difficulty of making in situ grazing measurements on mesozooplankton,

903   combined with the inherent uncertainty of these measurements can make it challenging to

904   differentiate between, for instance Ivlev and Holling's disk grazing formulations (e.g., Fig. 4 in

905 Morrow et al. (2018)). Nevertheless, differences in parameterizing grazing can lead to
906 substantially different model behavior (Anderson et al., 2010; Sailley et al., 2015; Wainwright et
907 al., 2007). In NEMURO-GoM, secondary production and dietary preferences of the
908 mesozooplankton community are both strongly influenced by model grazing formulation. While
909 we carefully chose parameterizations that gave reasonable fits to extensive field datasets of
910 zooplankton biomass and grazing rates, this does not preclude the possibility that other functional
911 forms would have more accurately simulated zooplankton dynamics. Hence, future PBMs should
912 investigate how different grazing formulations impact zooplankton dynamics in the region. We
913 especially recommend collaborations between experimentalists (potentially using new techniques
914 such as DNA metabarcoding of gut contents) and modelers to develop synthetic approaches with
915 the potential to quantitatively assess the realism of different grazing formulations.

916 Clear model-data mismatch is also evident in the proportion of grazing mediated by PZ and LZ.
917 This may be due to the fact that PZ is by default explicitly defined and parameterized as a higher
918 trophic level mesozooplankton that can feed on LZ. In reality, while there is a correlation between
919 size and trophic level in the ocean, many predatory zooplankton are <1 mm, and many suspension-
920 feeding zooplankton are >1 mm; hence, the overlap of taxonomic groups with different functional
921 roles and sizes makes it difficult to directly compare model categories to field data. For example,
922 shelf suspension-feeding zooplankton are likely larger than their counterparts in the oligotrophic
923 GoM although their functional role in the ecosystem does not change between environments.

924 The ecological impact of the model's potential overestimation of LZ grazing rates is most likely
925 to manifest through an increase in the ratio of secondary production to mesozooplankton biomass.
926 Since both LZ and PZ biomasses are accurately modeled by NEMURO-GoM, the overestimation
927 of grazing rates suggests that LZ turnover times may be too high, thus leading to higher estimates
928 of secondary production. However, this interpretation may oversimplify the complex interactions
929 within pelagic protistan communities. In the oligotrophic region where our model overestimates
930 LZ grazing rates, the model indicates that heterotrophic protists comprise approximately half of
931 the LZ diet. Thus, overestimates of grazing on LP do not necessarily lead to overestimates in total
932 consumption if <1-mm zooplankton derive substantial nutrition from non-phototrophic sources in
933 the field. Furthermore, the model's construction (i.e., LZ and PZ are functional groups, while the
934 field data are size classes) suggests that part of the model-data mismatch in Fig. 5d may result

935 from the presence of some suspension-feeders (i.e., LZ) in the >1-mm zooplankton size class and
936 some carnivorous zooplankton (i.e., PZ) in the <1-mm zooplankton size class. In this case, the
937 model may simply attribute too high of a LP:SZ prey ratio to LZ. If this is the issue, the model's
938 estimate of LZ secondary production may be accurate, but its trophic level too low (or, conversely,
939 the trophic level of PZ too high). Direct assessments of zooplankton trophic position (e.g., by
940 compound specific isotopic analysis of amino acids,(Chikaraishi et al., 2009; Décima et al., 2017)
941 may help resolve these issues.

4.3   Mesozooplankton dynamics in the open-ocean oligotrophic Gulf of Mexico

943 Despite its nutrient-poor conditions, the open-ocean GoM ecosystem is a key region for spawning
944 and larval development of many commercially important fishes, including Atlantic bluefin tuna,
945 yellowfin tuna, skipjack tuna, sailfish and mahi mahi (Cornic and Rooker, 2018; Kitchens and
946 Rooker, 2014; Lindo-Atichati et al., 2012; Muhling et al., 2017; Rooker et al., 2012, 2013). Why
947 so many species choose such oligotrophic waters as habitat for their larval stages is unknown, but
948 may be due to reduced predation risk (Bakun, 2013; Bakun and Broad, 2003). Regardless, rapid
949 growth and survival through the larval period depends on mesozooplankton prey that are suitably
950 abundant and appropriately sized for these larval fishes. These prey taxa may be especially
951 sensitive to increased stratification and oligotrophication associated with climate change, making
952 investigation of their dynamics and production an important topic of research.

953 Mesozooplankton biomass in the oligotrophic GoM was found to be strikingly low in both
954 observations and model estimates, approximately an order of magnitude less than on the shelf.
955 Model results clearly show that this low biomass condition arises from bottom-up resource
956 limitation. Our results suggest that low phytoplankton biomass in oligotrophic regions, and
957 particularly within Loop Current Eddies, may even lead to localized and episodic regions where
958 phytoplankton concentrations approach thresholds low enough that trigger collapse of
959 mesozooplankton grazing. Prey limiting conditions for mesozooplankton and their predators
960 would be expected more frequently in the GoM during warmer ocean conditions. Higher sea
961 surface temperatures and increased thermal stratification could suppress vertical mixing, resulting
962 in lower phytoplankton biomass.

Despite extreme oligotrophy and dominance of picophytoplankton, our model shows that both PZ and LZ can be sustained at modest abundances in the oligotrophic GoM. Indeed, the substantial abundances of large (>1 mm) mesozooplankton, equivalent to 60% of total mesozooplankton in both observations and model results (**Fig. 4A, C**), is an important result that helps explain the success of larval fish in the region. Our results show that large mesozooplankton (PZ) occupy a trophic position of approximately 3.0 in the open ocean GoM, which is marginally lower than on the shelf where they feed primarily on small mesozooplankton (LZ). The change in trophic position is associated with a switch from carnivory to feeding predominantly on heterotrophic protists in the oligotrophic region. This result highlights the importance of intermediate protistan trophic levels in sustaining mesozooplankton communities in oligotrophic regions. Indeed, both LZ and PZ ingest proportionally more SZ in the open ocean than on the shelf. Notably, these protistan trophic steps cannot be quantified by routine field techniques because they have no pigment signature to make them visible in gut pigment measurements and may not enrich in bulk ^{15}N leading to isotopic invisibility from a trophic perspective (Gutiérrez-Rodríguez et al., 2014). Despite their importance to phytoplankton grazing, they are sometimes missing from GoM ecosystem models (e.g., Fennel et al., 2011) and severely underrepresented or even absent in complex mass-balance constrained models (Arreguin-Sanchez et al., 2004; Geers et al., 2016). New insights may arise from focused investigations of phytoplankton➔protist➔crustacean linkages in oligotrophic regions in both model and experimental studies. This will likely require the use of next-generation technologies such as compound specific isotopic analyses of specific amino acids that have been shown to enrich in protists (Décima et al., 2017) or DNA metabarcoding to assess zooplankton gut contents (Cleary et al., 2016).

Another robust finding from this study is the dynamic mesoscale variability in zooplankton abundance, diet, and trophic position. These model results highlight the impact of Loop Current Eddies and mesoscale fronts and other features in modifying the biogeochemistry and food web of the GoM. The existence of hot spots of productivity in the GoM has been noted in observational studies (Biggs and Ressler, 2001), and the importance of GoM mesoscale features to fish larvae has been hypothesized (Domingues et al., 2016; Lindo-Atichati et al., 2012; Rooker et al., 2012). Indeed, cyclonic eddies were found to have enhanced secondary production in our model, while secondary production was depressed within anticyclonic eddies. Our results further suggest that these mesoscale structures may not only modify zooplankton abundances, but also their trophic

994 roles in the ecosystem, with implications for the transfer efficiencies of carbon and nitrogen in the
995 pelagic food web.

996 **5.0   Conclusions**

997 In this study we developed a PBM for the GoM and after extensive validation used the model to
998 investigate zooplankton community dynamics. The model was able to capture broad ecosystem
999 attributes including phytoplankton and mesozooplankton abundances, depth of the DCM and
1000 nutricline, as well as growth and grazing patterns. Based on model estimates of trophic position
1001 and diet our results suggest that on the shelf small mesozooplankton are strongly herbivorous while
1002 large mesozooplankton are strongly carnivorous. However, distinct changes in diet were noted in
1003 the oligotrophic GoM, where both groups rely more on protistan prey. Changes in diet and
1004 secondary production highlighted in this study have the potential to impact food availability to
1005 higher trophic levels, such as pelagic larval fishes. In future work, we plan to couple NEMURO-
1006 GoM to an individual-based model to evaluate the extent to which mesozooplankton abundance
1007 limits larval fish feeding, growth, and survival along transport pathways in the GoM. Insights from
1008 this ecosystem-based approach may help to better resolve stock-recruitment relationships that are
1009 needed for sustainable fisheries management and improved stock-assessment models.

1010

1011   *Code and data availability.*

1012   The model code and model validation data used in this study can be downloaded from GitHub at

1013   https://github.com/tashrops/NEMURO-GoM. An idealized one-dimensional version of

1014   NEMURO-GoM written in Matlab is also provided. The three-dimensional NEMURO-GoM

1015   model outputs used in the study are available on the FSU-COAPS server in a Network Common

1016   Data Form (NetCDF format). Data are also publicly available through the Gulf of Mexico Research

1017   Initiative Information and Data Cooperative (GRIIDC) at https://data.gulfresearchinitiative.org

1018   (doi: R6.X803.000:0018).

1019   *Author Contribution.*

1020   TAS conducted all numerical simulations and model analysis. EPC, SLM, and AB provided

1021   expertise on the hydrodynamic modeling. MRS and VJC provided expertise on the biogeochemical

1022   model coding and tuning. RS, MRS, MRL, and GZ processed and provided data that was central

1023   to NEMURO-GoM's validation. TAS wrote the manuscript with contributions from all authors.

1024   *Competing interest.*

1025   The authors declare that they have no conflict of interest

1026   *Acknowledgements.*

1027   We thank the captains and crew of the NOAA ship Nancy Foster and many of our colleagues from

1028   NOAA SEFSC and the NASA-funded Zooplankton from Space project. We thank Oliver Jahn for

1029   providing valuable direction in configuring the offline MITgcm package as well as Mandy

1030   Karnauskas, Sang-Ki Lee, and Fabian Gomez for their input during model development. We also

1031   thank Rémi Laxenaire for assistance with the TOEddies eddy detection algorithm. This paper is a

1032   result of research supported by The Gulf of Mexico Research Initiative under the CSOMIO project,

1033   the NOAA RESTORE Science Program under federal funding opportunity NOAA-NOS-NCCOS-

1034   2017-2004875, the NOAA Center for Coastal and Marine Ecosystems (NOAA Office of

1035   Education/Educational Partnership Program award NA16SEC48100009), the NOAA NMFS

1036   Fisheries and the Environment program, the Northern Gulf Institute (projects 18-NGI3-41 and 18-

1037   NGI3-52) under NOAA award NA06OAR4320264 06111039, and by NASA IDS grant

1038   #80NSSC17K0560.

References

Anderson, T. R.: Plankton functional type modelling: Running before we can walk?, J. Plankton Res., 27(11), 1073–1081, doi:10.1093/plankt/fbi076, 2005.

Anderson, T. R., Gentleman, W. C. and Sinha, B.: Influence of grazing formulations on the emergent properties of a complex ecosystem model in a global ocean general circulation model, Prog. Oceanogr., 87(1–4), 201–213, doi:10.1016/j.pocean.2010.06.003, 2010.

Anderson, T. R., Gentleman, W. C. and Yool, A.: EMPOWER-1.0: An Efficient Model of Planktonic ecOsystems WrittEn in R, Geosci. Model Dev., 8(7), 2231–2262, doi:10.5194/gmd-8-2231-2015, 2015.

Arreguin-Sanchez, F., Zetina-Rejón, M., Manickchand-Heileman, S., Ramírez-Rodríguez, M. and Vidal, L.: Simulated response to harvesting strategies in an exploited ecosystem in the southwestern Gulf of Mexico, Ecol. Modell., 172(2–4), 421–432, doi:10.1016/j.ecolmodel.2003.09.016, 2004.

Bakun, A.: Ocean eddies, predator pits and bluefin tuna: Implications of an inferred "low risk-limited payoff" reproductive scheme of a (former) archetypical top predator, Fish Fish., 14(3), 424–438, doi:10.1111/faf.12002, 2013.

Bakun, A. and Broad, K.: Environmental "loopholes" and fish population dynamics: Comparative pattern recognition with focus on El Niño effects in the Pacific, Fish. Oceanogr., 12(4–5), 458–473, doi:10.1046/j.1365-2419.2003.00258.x, 2003.

Biggs, D. C. and Ressler, P. H.: Distribution and abundance of phytoplankton, zooplankton, icthyoplankton, and micronekton in the deepwater Gulf of Mexico, Gulf Mex. Sci., 2001(1), 7–29, doi:10.18785/goms.1901.02, 2001.

Buitenhuis, E., Le Quere, C., Aumont, O., Beaugrand, G., Bunker, A., Hirst, A., Ikeda, T., T, O. B., Piontkovski, S. and Straile, D.: Biogeochemical fluxes through mesozooplankton - art. no. GB2003, Global Biogeochem. Cycles, 20 (2), NIL_1-NIL_18, doi:10.1029/2005GB002511, 2006.

Calbet, A.: Mesozooplankton grazing effect on primary production: A global comparative analysis in marine ecosystems, Limnol. Oceanogr., 46(7), 1824–1830, doi:10.4319/lo.2001.46.7.1824, 2001.

Caron, D. A. and Hutchins, D. A.: The effects of changing climate on microzooplankton grazing and community structure: Drivers, predictions and knowledge gaps, J. Plankton Res., 35(2), 235–252, doi:10.1093/plankt/fbs091, 2013.

Chaigneau, A., Le Texier, M., Eldin, G., Grados, C. and Pizarro, O.: Vertical structure of mesoscale eddies in the eastern South Pacific Ocean: A composite analysis from altimetry and Argo profiling floats, J. Geophys. Res. Ocean., 116(11), 1–16, doi:10.1029/2011JC007134, 2011.

Chassignet, E. P., Smith, L. T., Halliwell, G. R. and Bleck, R.: North Atlantic simulations with the Hybrid Coordinate Ocean Model (HYCOM): Impact of the vertical coordinate choice, reference pressure, and thermobaricity, J. Phys. Oceanogr., 33(12), 2504–2526, doi:10.1175/1520-0485(2003)033<2504:NASWTH>2.0.CO;2, 2003.

1080 Chikaraishi, Y., Ogawa, N. O., Kashiyama, Y., Takano, Y., Suga, H., Tomitani, A., Miyashita,
1081 H., Kitazato, H. and Ohkouchi, N.: Chikaraishi_et_al-2009-
1082 Limnology_and_Oceanography%3A_Methods, , (2003), 740–750, 2009.

1083 Cleary, A. C., Durbin, E. G., Rynearson, T. A. and Bailey, J.: Feeding by Pseudocalanus
1084 copepods in the Bering Sea: Trophic linkages and a potential mechanism of niche partitioning,
1085 Deep. Res. Part II Top. Stud. Oceanogr., 134, 181–189, doi:10.1016/j.dsr2.2015.04.001, 2016.

1086 Coles, V. J., Stukel, M. R., Brooks, M. T., Burd, A., Crump, B. C., Moran, M. A., Paul, J. H.,
1087 Satinsky, B. M., Yager, P. L., Zielinski, B. L. and Hood, R. R.: Ocean biogeochemistry modeled
1088 with emergent trait-based genomics, Science (80-.)., 358(6367), 1149–1154,
1089 doi:10.1126/science.aan5712, 2017.

1090 Cornic, M. and Rooker, J. R.: Influence of oceanographic conditions on the distribution and
1091 abundance of blackfin tuna (Thunnus atlanticus) larvae in the Gulf of Mexico, Fish. Res.,
1092 201(July 2017), 1–10, doi:10.1016/j.fishres.2017.12.015, 2018.

1093 Damien, P., Pasqueron de Fommervault, O., Sheinbaum, J., Jouanno, J., Camacho-Ibar, V. F. and
1094 Duteil, O.: Partitioning of the Open Waters of the Gulf of Mexico Based on the Seasonal and
1095 Interannual Variability of Chlorophyll Concentration, J. Geophys. Res. Ocean., 123(4), 2592–
1096 2614, doi:10.1002/2017JC013456, 2018.

1097 Decima, M., Landry, M. R., Stukel, M. R., Lopez-Lopez, L. and Krause, J. W.:
1098 Mesozooplankton biomass and grazing in the Costa Rica Dome: Amplifying variability through
1099 the plankton food web, J. Plankton Res., 38(2), 317–330, doi:10.1093/plankt/fbv091, 2016.

1100 Décima, M., Landry, M. R. and Rykaczewski, R. R.: Broad scale patterns in mesozooplankton
1101 biomass and grazing in the eastern equatorial Pacific, Deep. Res. Part II Top. Stud. Oceanogr.,
1102 58(3–4), 387–399, doi:10.1016/j.dsr2.2010.08.006, 2011.

1103 Décima, M., Landry, M. R., Bradley, C. J. and Fogel, M. L.: Alanine δ15N trophic fractionation
1104 in heterotrophic protists, Limnol. Oceanogr., 62(5), 2308–2322, doi:10.1002/lno.10567, 2017.

1105 Domingues, R., Goni, G., Bringas, F., Muhling, B., Lindo-Atichati, D. and Walter, J.: Variability
1106 of preferred environmental conditions for Atlantic bluefin tuna (Thunnus thynnus) larvae in the
1107 Gulf of Mexico during 1993-2011, Fish. Oceanogr., 25(3), 320–336, doi:10.1111/fog.12152,
1108 2016.

1109 Doney, S. C., Lima, I., Moore, J. K., Lindsay, K., Behrenfeld, M. J., Westberry, T. K.,
1110 Mahowald, N., Glover, D. M. and Takahashi, T.: Skill metrics for confronting global upper
1111 ocean ecosystem-biogeochemistry models against field and remote sensing data, J. Mar. Syst.,
1112 76(1–2), 95–112, doi:10.1016/j.jmarsys.2008.05.015, 2009.

1113 Everett, J. D., Baird, M. E., Buchanan, P., Bulman, C., Davies, C., Downie, R., Griffiths, C.,
1114 Heneghan, R., Kloser, R. J., Laiolo, L., Lara-Lopez, A., Lozano-Montes, H., Matear, R. J.,
1115 McEnnulty, F., Robson, B., Rochester, W., Skerratt, J., Smith, J. A., Strzelecki, J., Suthers, I. M.,
1116 Swadling, K. M., van Ruth, P. and Richardson, A. J.: Modeling what we sample and sampling
1117 what we model: Challenges for zooplankton model assessment, Front. Mar. Sci., 4(MAR), 1–19,
1118 doi:10.3389/fmars.2017.00077, 2017.

1119 Fasham, M. J. R., Ducklow, H. W. and McKelvie, S. M.: A nitrogen-based model of plankton
1120 dynamics in the ocean mixed layer, J. Mar. Res., 48(3), 591–639, 1990.

Fennel, K., Wilkin, J., Levin, J., Moisan, J., O'Reilly, J. and Haidvogel, D.: Nitrogen cycling in the Middle Atlantic Bight: Results from a three-dimensional model and implications for the North Atlantic nitrogen budget, Global Biogeochem. Cycles, 20(3), 1–14, doi:10.1029/2005GB002456, 2006.

Fennel, K., Hetland, R., Feng, Y. and Dimarco, S.: A coupled physical-biological model of the Northern Gulf of Mexico shelf: Model description, validation and analysis of phytoplankton variability, Biogeosciences, 8(7), 1881–1899, doi:10.5194/bg-8-1881-2011, 2011.

Follows, M. J., Dutkiewicz, S., Grant, S. and Chisholm, S. W.: Emergent biogeography of microbial communities in a model ocean., Science, 315(5820), 1843–1846, doi:10.1126/science.1138544, 2007.

Forristall, G. Z., Schaudt, K. J. and Cooper, C. K.: Evolution and kinematics of a loop current eddy in the Gulf of Mexico during 1985, J. Geophys. Res., 97(C2), 2173, doi:10.1029/91jc02905, 1992.

Franks, P. J. S.: NPZ models of plankton dynamics: Their construction, coupling to physics, and application, J. Oceanogr., 58(2), 379–387, doi:10.1023/A:1015874028196, 2002.

Franks, P. J. S.: Planktonic ecosystem models: Perplexing parameterizations and a failure to fail, J. Plankton Res., 31(11), 1299–1306, doi:10.1093/plankt/fbp069, 2009.

Geers, T. M., Pikitch, E. K. and Frisk, M. G.: An original model of the northern Gulf of Mexico using Ecopath with Ecosim and its implications for the effects of fishing on ecosystem structure and maturity, Deep. Res. Part II Top. Stud. Oceanogr., 129, 319–331, doi:10.1016/j.dsr2.2014.01.009, 2016.

Geiderl, R. J., Maclntyre, H. L. and Kana, T. M.: A dynamic regulatory model of phytoplanktonic acclimation to light, nutrients, and temperature, Limnol. Ocean., 43(4), 679–694, doi:10.4319/lo.1998.43.4.0679, 1998.

Gentleman, W., Leising, A., Frost, B., Strom, S. and Murray, J.: Functional responses for zooplankton feeding on multiple resources : a review of assumptions and biological dynamics, , 50, 2847–2875, doi:10.1016/j.dsr2.2003.07.001, 2003a.

Gentleman, W., Leising, A., Frost, B., Strom, S. and Murray, J.: Functional responses for zooplankton feeding on multiple resources: A review of assumptions and biological dynamics, Deep. Res. Part II Top. Stud. Oceanogr., 50(22–26), 2847–2875, doi:10.1016/j.dsr2.2003.07.001, 2003b.

Gentleman, W. C. and Neuheimer, A. B.: Functional responses and ecosystem dynamics: How clearance rates explain the influence of satiation, food-limitation and acclimation, J. Plankton Res., 30(11), 1215–1231, doi:10.1093/plankt/fbn078, 2008.

Gomez, F. A., Lee, S. K., Liu, Y., Hernandez, F. J., Muller-Karger, F. E. and Lamkin, J. T.: Seasonal patterns in phytoplankton biomass across the northern and deep Gulf of Mexico: A numerical model study, Biogeosciences, 15(11), 3561–3576, doi:10.5194/bg-15-3561-2018, 2018.

Gregg, W. W., Ginoux, P., Schopf, P. S. and Casey, N. W.: Phytoplankton and iron: Validation of a global three-dimensional ocean biogeochemical model, Deep. Res. Part II Top. Stud. Oceanogr., 50(22–26), 3143–3169, doi:10.1016/j.dsr2.2003.07.013, 2003.

Gutiérrez-Rodríguez, A., Décima, M., Popp, B. N. and Landry, M. R.: Isotopic invisibility of protozoan trophic steps in marine food webs, Limnol. Oceanogr., 59(5), 1590–1598, doi:10.4319/lo.2014.59.5.1590, 2014.

Holl, C. M., Waite, A. M., Pesant, S., Thompson, P. A. and Montoya, J. P.: Unicellular diazotrophy as a source of nitrogen to Leeuwin Current coastal eddies, Deep. Res. Part II Top. Stud. Oceanogr., 54(8–10), 1045–1054, doi:10.1016/j.dsr2.2007.02.002, 2007.

Hu, C., Lee, Z. and Franz, B.: Chlorophyll a algorithms for oligotrophic oceans: A novel approach based on three-band reflectance difference, J. Geophys. Res. Ocean., 117(1), 1–25, doi:10.1029/2011JC007395, 2012.

Ikeda, T., Kanno, Y., Ozaki, K. and Shinada, A.: Metabolic rates of epipelagic marine copepods as a function of body mass and temperature, Mar. Biol., 139(3), 587–596, doi:10.1007/s002270100608, 2001.

Kishi, M. J., Kashiwai, M., Ware, D. M., Megrey, B. a., Eslinger, D. L., Werner, F. E., Noguchi-Aita, M., Azumaya, T., Fujii, M., Hashimoto, S., Huang, D., Iizumi, H., Ishida, Y., Kang, S., Kantakov, G. a., Kim, H. C., Komatsu, K., Navrotsky, V. V., Smith, S. L., Tadokoro, K., Tsuda, A., Yamamura, O., Yamanaka, Y., Yokouchi, K., Yoshie, N., Zhang, J., Zuenko, Y. I. and Zvalinsky, V. I.: NEMURO-a lower trophic level model for the North Pacific marine ecosystem, Ecol. Modell., 202(1–2), 12–25, doi:10.1016/j.ecolmodel.2006.08.021, 2007.

Kitchens, L. L. and Rooker, J. R.: Habitat associations of dolphinfish larvae in the Gulf of Mexico, Fish. Oceanogr., 23(6), 460–471, doi:10.1111/fog.12081, 2014.

Kjellerup, S., Dünweber, M., Swalethorp, R., Nielsen, T. G., Møller, E. F., Markager, S. and Hansen, B. W.: Effects of a future warmer ocean on the coexisting copepods Calanus finmarchicus and C. glacialis in Disko Bay, western Greenland, Mar. Ecol. Prog. Ser., 447, 87–108, doi:10.3354/meps09551, 2012.

Landry, M., Haas, L. and Fagerness, V.: Dynamics of microbial plankton communities: experiments in Kaneohe Bay, Hawaii, Mar. Ecol. Prog. Ser., 16, 127–133, doi:10.3354/meps016127, 1984.

Landry, M. R. and Calbet, A.: Microzooplankton production in the oceans, ICES J. Mar. Sci., 61(4), 501–507, doi:10.1016/j.icesjms.2004.03.011, 2004.

Landry, M. R. and Hassett, R. P.: Estimating the grazing impact of marine micro-zooplankton, Mar. Biol., 67(3), 283–288, doi:10.1007/BF00397668, 1982.

Landry, M. R., Decima, M., Simmons, M. P., Hannides, C. C. S. and Daniels, E.: Mesozooplankton biomass and grazing responses to Cyclone Opal, a subtropical mesoscale eddy, Deep. Res. Part II Top. Stud. Oceanogr., 55(10–13), 1378–1388, doi:10.1016/j.dsr2.2008.01.005, 2008.

Landry, M. R., Ohman, M. D., Goericke, R., Stukel, M. R. and Tsyrklevich, K.: Lagrangian studies of phytoplankton growth and grazing relationships in a coastal upwelling ecosystem off Southern California, Prog. Oceanogr., 83(1–4), 208–216, doi:10.1016/j.pocean.2009.07.026, 2009.

Landry, M. R., Selph, K. E., Decima, M., Gutierrez-Rodríguez, A., Stukel, M. R., Taylor, A. G. and Pasulka, A. L.: Phytoplankton production and grazing balances in the Costa Rica Dome, J.

Plankton Res., 38(2), 366–379, doi:10.1093/plankt/fbv089, 2016.

Landry, M. R., Beckley, L. E. and Muhling, B. A.: Climate sensitivities and uncertainties in food-web pathways supporting larval bluefin tuna in subtropical oligotrophic oceans, ICES J. Mar. Sci., 76(2), 359–369, doi:10.1093/icesjms/fsy184, 2019.

Large, W. G., McWilliams, J. C. and Doney, S. C.: Oceanic vertical mixing: A review and a model with a nonlocal boundary layer parameterization, Rev. Geophys., 32(4), 363–403, doi:10.1029/94RG01872, 1994.

Laxenaire, R., Speich, S., Blanke, B., Chaigneau, A., Pegliasco, C. and Stegner, A.: Anticyclonic Eddies Connecting the Western Boundaries of Indian and Atlantic Oceans, J. Geophys. Res. Ocean., 123(11), 7651–7677, doi:10.1029/2018JC014270, 2018.

Laxenaire, R., Speich, S. and Stegner, A.: Evolution of the Thermohaline Structure of One Agulhas Ring Reconstructed from Satellite Altimetry and Argo Floats, J. Geophys. Res. Ocean., 124(12), 8969–9003, doi:10.1029/2018JC014426, 2019.

Li, Q. P., Franks, P. J. S., Landry, M. R., Goericke, R. and Taylor, A. G.: Modeling phytoplankton growth rates and chlorophyll to carbon ratios in California coastal and pelagic ecosystems, J. Geophys. Res. Biogeosciences, 115(4), 1–12, doi:10.1029/2009JG001111, 2010.

Lindo-Atichati, D., Bringas, F., Goni, G., Muhling, B., Muller-Karger, F. E. and Habtes, S.: Varying mesoscale structures influence larval fish distribution in the northern Gulf of Mexico, Mar. Ecol. Prog. Ser., 463, 245–257, doi:10.3354/meps09860, 2012.

Maul, G. A. and Vukovich, F. M.: The Relationship between Variations in the Gulf of Mexico Loop Current and Straits of Florida Volume Transport, , 785–796, 1993.

McKinley, G. A., Follows, M. J. and Marshall, J.: Mechanisms of air-sea CO2 flux variability in the equatorial Pacific and the North Atlantic, Global Biogeochem. Cycles, 18(2), 1–14, doi:10.1029/2003GB002179, 2004.

Mitra, A., Flynn, K. J., Burkholder, J. M., Berge, T., Calbet, A., Raven, J. A., Granéli, E., Glibert, P. M., Hansen, P. J., Stoecker, D. K., Thingstad, F., Tillmann, U., Väge, S., Wilken, S. and Zubkov, M. V.: The role of mixotrophic protists in the biological carbon pump, Biogeosciences, 11(4), 995–1005, doi:10.5194/bg-11-995-2014, 2014.

Moeller, H. V., Laufkötter, C., Sweeney, E. M. and Johnson, M. D.: Light-dependent grazing can drive formation and deepening of deep chlorophyll maxima, Nat. Commun., 10(1), doi:10.1038/s41467-019-09591-2, 2019.

Morey, S. L., Martin, P. J., O'Brien, J. J., Wallcraft, A. A. and Zavala-Hidalgo, J.: Export pathways for river discharged fresh water in the northern Gulf of Mexico, J. Geophys. Res. C Ocean., 108(10), 1–1, doi:10.1029/2002jc001674, 2003a.

Morey, S. L., Schroeder, W. W., O'Brien, J. J. and Zavala-Hidalgo, J.: The annual cycle of riverine influence in the eastern Gulf of Mexico basin, Geophys. Res. Lett., 30(16), doi:10.1029/2003GL017348, 2003b.

Morey, S. L., Zavala-Hidalgo, J. and O'Brien, J. J.: The Seasonal Variability of Continental Shelf Circulation in the Northern and Western Gulf of Mexico from a High-Resolution Numerical Model, in Circulation in the Gulf of Mexico: Observations and Models, vol. 161, pp. 203–218., 2013.

Morrow, R. M., Ohman, M. D., Goericke, R., Kelly, T. B., Stephens, B. M. and Stukel, M. R.: CCE V: Primary production, mesozooplankton grazing, and the biological pump in the California Current Ecosystem: Variability and response to El Niño, Deep. Res. Part I Oceanogr. Res. Pap., 140(June), 52–62, doi:10.1016/j.dsr.2018.07.012, 2018.

Muhling, B. A., Lamkin, J. T., Alemany, F., García, A., Farley, J., Ingram, G. W., Berastegui, D. A., Reglero, P. and Carrion, R. L.: Reproduction and larval biology in tunas, and the importance of restricted area spawning grounds., 2017.

Mulholland, M. R., Bernhardt, P. W., Heil, C. A., Bronk, D. A. and O'Neil, J. M.: Nitrogen fixation and release of fixed nitrogen by Trichodesmium spp. in the Gulf of Mexico, Limnol. Oceanogr., 51(5), 2484, doi:10.4319/lo.2006.51.5.2484, 2006.

Murray, A. G. and Parslow, J. S.: The analysis of alternative formulations in a simple model of a coastal ecosystem, Ecol. Modell., 119(2–3), 149–166, doi:10.1016/S0304-3800(99)00046-0, 1999.

Oey, L., Ezer, T. and Lee, H.: Loop Current, rings and related circulation in the Gulf of Mexico: A review of numerical …, Geophys. Monogr. …, 161, 31–56 [online] Available from: http://scholar.google.com/scholar?cites=642048877832323420&hl=en#46, 2005.

Parker, R. A.: Dynamic models for ammonium inhibition of nitrate uptake by phytoplankton, Ecol. Modell., doi:10.1016/0304-3800(93)90042-Q, 1993.

Pegliasco, C., Chaigneau, A. and Morrow, R.: Main eddy vertical structures observed in the four major Eastern Boundary Upwelling Systems, J. Geophys. Res. Ocean., 120(9), 6008–6033, doi:10.1002/2015JC010950, 2015.

Pörtner, H. O. and Farrell, A. P.: Physiology and Climate Change Hans, Science (80-.)., 322(October), 690–692 [online] Available from: http://epic.awi.de/epic/Main?puid=32305&lang=en, 2008.

Richardson, A. J.: In hot water: Zooplankton and climate change, ICES J. Mar. Sci., 65(3), 279–295, doi:10.1093/icesjms/fsn028, 2008.

Riley, G. A.: Factors controlling phytoplankton populations on Georges Bank, J. Mar. Res., 6(1), 54–73, 1946.

Rooker, J. R., Simms, J. R., David Wells, R. J., Holt, S. A., Holt, G. J., Graves, J. E. and Furey, N. B.: Distribution and habitat associations of billfish and swordfish larvae across mesoscale features in the gulf of Mexico, PLoS One, 7(4), doi:10.1371/journal.pone.0034180, 2012.

Rooker, J. R., Kitchens, L. L., Dance, M. A., Wells, R. J. D., Falterman, B. and Cornic, M.: Spatial, Temporal, and Habitat-Related Variation in Abundance of Pelagic Fishes in the Gulf of Mexico: Potential Implications of the Deepwater Horizon Oil Spill, PLoS One, 8(10), doi:10.1371/journal.pone.0076080, 2013.

Sailley, S. F., Vogt, M., Doney, S. C., Aita, M. N., Bopp, L., Buitenhuis, E. T., Hashioka, T., Lima, I., Le Quéré, C. and Yamanaka, Y.: Comparing food web structures and dynamics across a suite of global marine ecosystem models, Ecol. Modell., 261–262, 43–57, doi:10.1016/j.ecolmodel.2013.04.006, 2013.

Sailley, S. F., Polimene, L., Mitra, A., Atkinson, A. and Allen, J. I.: Impact of zooplankton food selectivity on plankton dynamics and nutrient cycling, J. Plankton Res., 37(3), 519–529,

1285   doi:10.1093/plankt/fbv020, 2015.

1286   Selph, K. E., Landry, M. R., Taylor, A. G., Gutierrez-Rodríguez, A., Stukel, M. R., Wokuluk, J.
1287   and Pasulka, A.: Phytoplankton production and taxon-specific growth rates in the Costa Rica
1288   Dome, J. Plankton Res., 38(2), 199–215, doi:10.1093/plankt/fbv063, 2016.

1289   Sherr, E. B. and Sherr, B. F.: Significance of predation by protists in aquatic microbial food
1290   webs, Antonie van Leeuwenhoek, Int. J. Gen. Mol. Microbiol., 81(1–4), 293–308,
1291   doi:10.1023/A:1020591307260, 2002.

1292   Staniewski, M. A. and Short, S. M.: Methodological review and meta-analysis of dilution assays
1293   for estimates of virus- and grazer-mediated phytoplankton mortality, Limnol. Oceanogr.
1294   Methods, 16(10), 649–668, doi:10.1002/lom3.10273, 2018.

1295   Steele, J. H. and Henderson, E. W.: The role of predation in plankton models, J. Plankton Res.,
1296   doi:10.1093/plankt/14.1.157, 1992.

1297   Steinberg, D. K. and Landry, M. R.: Zooplankton and the Ocean Carbon Cycle, Ann. Rev. Mar.
1298   Sci., 9(1), 413–444, doi:10.1146/annurev-marine-010814-015924, 2017.

1299   Straile, D.: and metazoan efficiencies of protozoan Gross growth on food concentration , and
1300   their dependence zooplankton group ratio , and taxonomic, Limnol. Oceanogr., 42(6), 1375–
1301   1385, 1997.

1302   Strickland, J. D. H. and Parsons., T. R.: A practical handbook for seawater analysis. Second
1303   Edition. [online] Available from: http://www.dfo-mpo.gc.ca/Library/1507.pdf, 1972.

1304   Strom, S. L., Benner, R., Ziegler, S. and Dagg, M. J.: Planktonic grazers are a potentially
1305   important source of marine dissolved organic carbon, Limnol. Oceanogr., 42(6), 1364–1374,
1306   doi:10.4319/lo.1997.42.6.1364, 1997.

1307   Stukel, M. R., Coles, V. J., Brooks, M. T. and Hood, R. R.: Top-down, bottom-up and physical
1308   controls on diatom-diazotroph assemblage growth in the Amazon River plume, Biogeosciences,
1309   11(12), 3259–3278, doi:10.5194/bg-11-3259-2014, 2014.

1310   Stukel, M. R., Kahru, M., Benitez-Nelson, C. R., Décima, M., Goericke, R., Landry, M. R. and
1311   Ohman, M. D.: Using Lagrangian-based process studies to test satellite algorithms of vertical
1312   carbon flux in the eastern North Pacific Ocean, J. Geophys. Res. Ocean., 120(11), 7208–7222,
1313   doi:10.1002/2015JC011264, 2015.

1314   Turner, J. T.: Zooplankton fecal pellets, marine snow, phytodetritus and the ocean's biological
1315   pump, Prog. Oceanogr., 130, 205–248, doi:10.1016/j.pocean.2014.08.005, 2015.

1316   Werner, F. E., Ito, S. I., Megrey, B. A. and Kishi, M. J.: Synthesis of the NEMURO model
1317   studies and future directions of marine ecosystem modeling, Ecol. Modell., 202(1–2), 211–223,
1318   doi:10.1016/j.ecolmodel.2006.08.019, 2007.

1319   Xue, Z., He, R., Fennel, K., Cai, W. J., Lohrenz, S. and Hopkinson, C.: Modeling ocean
1320   circulation and biogeochemical variability in the Gulf of Mexico, Biogeosciences, 10(11), 7219–
1321   7234, doi:10.5194/bg-10-7219-2013, 2013.

1322